ELASTIC PROPERTIES OF BORON SUBOXIDE AND THE DIAMETRICAL COMPRESSION OF BRITTLE SPHERES

Daniel R. Petrak, et al

Air Force Materials Laboratory
Wright-Patterson Air Force Base, Ohio

June 1973

AFML-TR-73-84

ELASTIC PROPERTIES OF BORON SUBOXIDE AND THE DIAMETRICAL COMPRESSION OF BRITTLE SPHERES

DANIEL R. PETRAK AND ROBERT RUH
AND
WILLIAM B. SHOOK

OHIO STATE UNIVERSITY
COLUMBUS, OHIO

TECHNICAL REPORT AFML-TR-73-84

JUNE 1973

AIR FORCE MATERIALS LABORATORY
AIR FORCE SYSTEMS COMMAND
WRIGHT-PATTERSON AIR FORCE BASE, OHIO

NOTICE

When Government drawings, specifications, or other data are used for any purpose other than in connection with a definitely related Government procurement operation, the United States Government thereby incurs no responsibility nor any obligation whatsoever; and the fact that the government may have formulated, furnished, or in any way supplied the said drawings, specifications, or other data, is not to be regarded by implication or otherwise as in any manner licensing the holder or any other person or corporation, or conveying any rights or permission to manufacture, use, or sell any patented invention that may in any way be related thereto.

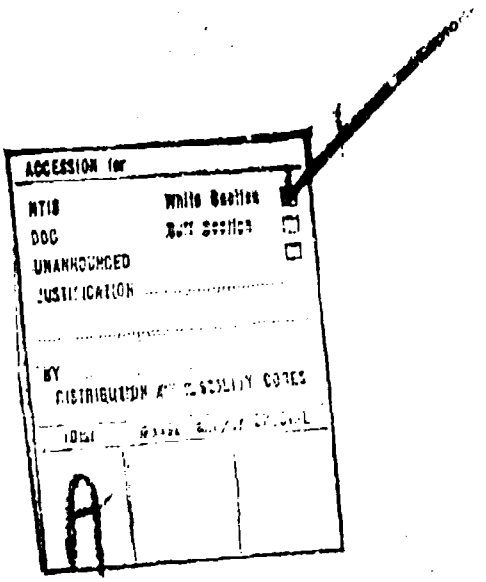

Copies of this report should not be returned unless return is required by security considerations, contractual obligations, or notice on a specific document.

AIR FORCE/56/80/25 July 1973 — 200

ELASTIC PROPERTIES OF BORON SUBOXIDE AND THE DIAMETRICAL COMPRESSION OF BRITTLE SPHERES

DANIEL R. PETRAK AND ROBERT RUH

AND

WILLIAM B. SHOOK

/ 2.

FOREWORD

This report was prepared by Daniel R. Petrak and Robert Ruh, Metals and Ceramics Synthesis Branch, Metals and Ceramics Division, Air Force Materials Laboratory and William B. Shook, Department of Ceramic Engineering, Ohio State University, Columbus, Ohio. The work was conducted under Project 7350, "Refractory Inorganic Nonmetallic Materials."

The research was conducted during the period June 1971 to June 1972.

The authors wish to acknowledge the following for their contributions during the course of this investigation. Lt. G. W. Hollenberg of AFML and Mr. G. Petrak, University of Dayton Research Institute for stimulating discussions and encouragement, Mr. C. E. Smith and Mr. V. A. Patel for assistance in the preparation of specimens, Mr. E. Strader of the University of Dayton Research Institute for assistance in the high speed photography studies and Mrs. J. Gwinn for preparation of the manuscript.

This technical report has been reviewed and is approved.

C. M. PIERCE, Acting Chief
Metal and Ceramic Synthesis Group
Metals and Ceramics Division
Air Force Materials Laboratory

UNCLASSIFIED
Security Classification

AD-764355

DOCUMENT CONTROL DATA - R & D

(Security classification of title, body of abstract and indexing annotation must be entered when the overall report is classified)

1. ORIGINATING ACTIVITY (Corporate author)
Air Force Materials Laboratory
Wright-Patterson Air Force Base, Ohio 45433

2a. REPORT SECURITY CLASSIFICATION
Unclassified

2b. GROUP

3. REPORT TITLE
Elastic Properties of Boron Suboxide and the Diametrical Compression of Brittle Spheres

4. DESCRIPTIVE NOTES (Type of report and inclusive dates)

5. AUTHOR(S) (First name, middle initial, last name)
Daniel R. Petrak, Robert Ruh, and William B. Shook

6. REPORT DATE	7a. TOTAL NO OF PAGES	7b. NO OF REFS
June 1973	~~102~~ 49	44

8a. CONTRACT OR GRANT NO	9a. ORIGINATOR'S REPORT NUMBER(S)
b. PROJECT NO 7350	AFML-TR-73-84
c. Task 735001	9b. OTHER REPORT NO(S) (Any other numbers that may be assigned this report)
d.	

10. DISTRIBUTION STATEMENT
Approved for public release; distribution unlimited

11. SUPPLEMENTARY NOTES	12. SPONSORING MILITARY ACTIVITY
	Air Force Materials Laboratory Wright-Patterson AFB, Ohio

13. ABSTRACT

The room temperature elastic moduli of hot pressed boron suboxide were determined in the 0-16% porosity range using the resonant sphere technique. Results revealed that Poisson's ratio was constant in this range and that Young's and shear moduli followed Hasselman's semi-empirical relation with E_o = 68.5 x 10^6 psi and A = 5.1. High speed photographs of diametrically compressed glass spheres indicate that fracture initiates near the center of the sphere. Also a stress analysis of such a sphere shows that the maximum tensile stress occurs near the center of the sphere. Therefore a new test for the tensile strength of brittle materials is suggested which is not influenced by surface defects. The tensile strength of boron suboxide was determined using the diametrical compression test and values approximately 25% lower than four point bend tests were obtained.

DD FORM 1 NOV 65 1473

/ cc

UNCLASSIFIED
Security Classification

UNCLASSIFIED
Security Classification

14 KEY WORDS	LINK A		LINK B		LINK C	
	ROLE	WT	ROLE	WT	ROLE	WT
Boron suboxide						
Elastic properties						
Diametrical compression						
Tensile strength						

S/N Government Printing Office: 1973 — 759-495/640

UNCLASSIFIED
Security Classification

ABSTRACT

The room temperature elastic moduli of hot pressed boron suboxide were determined in the 0-16% porosity range using the resonant sphere technique. Results revealed that Poisson's ratio was constant in this range and that Young's and shear moduli followed Hasselman's semi-empirical relation with $E_o = 68.5 \times 10^6$ psi and $A = 5.1$. High speed photographs of diametrically compressed glass spheres indicate that fracture initiates near the center of the sphere. Also a stress analysis of such a sphere shows that the maximum tensile stress occurs near the center of the sphere. Therefore a new test for the tensile strength of brittle materials is suggested which is not influenced by surface defects. The tensile strength of boron suboxide was determined using the diametrical compression test and values approximately 25% lower than four point bend tests were obtained.

TABLE OF CONTENTS

ILLUSTRATIONS

TABLES

1. Introduction

The subject of impact physics has received considerable interest in the past ten years, particularly in regard to ceramic armor. A number of publications are available which suggest the importance of various properties for ceramic armor materials. The properties most commonly considered are microhardness, compressive strength, tensile strength, elastic impedance (density x longitudinal sound velocity) and the Hugoniot elastic limit. These are normally considered only as indicators however; the only conclusive test of a candidate ceramic armor material is actual ballistic testing.

The relatively high values of compressive strength and elastic impedance inherent in materials such as dense boron carbide, silicon carbide and aluminum oxide make them attractive materials for this application. Because armor is used parasitically (e.g., body armor), the density of the armor becomes important. Boron carbide, with a low theoretical density of 2.52 gm/cc^3, definitely has the advantage over most other ceramics. It has generally been considered as the best of the materials readily available. When economic factors become important though, aluminum oxide and silicon carbide based materials should normally be considered.

One of the two main topics of investigation in the present work was the determination of elastic properties of boron suboxide. This work was initiated as part of a characterization study of the material

in regard to ceramic armor and other structural applications. One stimulus for interest in boron suboxide was its extremely high microhardness reported by Rizzo et al.[20] Porosity is the single most important parameter which effects elastic properties. For this reason a knowledge of the dependence of elastic modulus on porosity was necessary for the consideration of any structural application.

It has been shown by flash X-ray photography that the failure of ceramic armor is not only a compressive one at the surface of impact but also a tensile failure is initiated near the back surface of the ceramic. This tensile failure is generated by the reflection of a compressive wave. The reflection is due to the elastic impedance mismatch between the ceramic and the backing material. The initiation of the tensile failure occurs beneath the surface of the ceramic.

Some investigators[42] have considered the failure at the back surface to be the limiting condition for conventional ceramic armor materials. They have attempted to deal with this problem by adding ductility to the ceramic by the addition of a metallic phase near the back surface. These materials have been termed gradient armor. Because of fabrication problems and usually an increase in density of the armor, these attempts have met with little success.

The second topic of investigation in the present work has been to propose a new test method for tensile strength which may be useful in the evaluation of materials with regard to the tensile failure in ceramic armor. All the currently used tests for tensile strength in brittle materials involve (or at least must allow for) fracture initiation at a surface. As will be demonstrated later, the diametral compression of a properly loaded sphere will initiate a tensile failure within the surface of the specimen.

The two topics covered in this work may, at first, appear to be somewhat unrelated. Use of the resonant sphere technique for the determination of elastic properties provides a spherical specimen which can then be tested for tensile strength. These procedures may be particularly convenient when only small specimens are available (i.e., spheres as small as 5 mm in diameter can be tested).

2. Literature Survey

2-1 Effect of Porosity on Elastic Moduli

The first attempt to predict the effect of porosity on elastic properties of materials was due to Mackenzie[1] who considered spherical pores in a homogeneous solid. The following relationships were derived:

$$1 - \frac{G}{G_o} = \frac{5(3K_o + 4G_o)}{(9K_o + 8G_o)} P + AP^2 \qquad 2\text{-}1$$

$$\frac{1}{K} = \frac{1}{K_o(1-P)} + \frac{3P}{4G_o(1-P)} + BP^3 \qquad 2\text{-}2$$

where G_o and K_o are the shear and bulk moduli, respectively, of the solid and P is the volume fraction porosity. A and B are coefficients of higher powers of P not determined by Mackenzie. The terms containing higher powers of P should have little effect at $P << 1$.

Coble and Kingery[2] attempted to evaluate the coefficient A in Equation (2-1) experimentally. Shear moduli data for porous alumina were fit to Equation (2-1) assuming Poisson's ratio equal to 0.3 and $K_o/G_o = 2.16$ and the boundary conditions $G = G_o$ at $P = 0$ and $G = 0$ at $P = 1$. Their experimental data showed good agreement for $A = -0.9$. Large discrepancies were noted however on data for other materials.

The theory given by Mackenzie produces equations for G and K. In order to calculate E, Young's modulus, the following relation

should be used:

$$E = \frac{9KG}{3K+C} \qquad 2\text{-}3$$

For equations interrelating all six elastic moduli see Appendix 1.

Using a cubic inclusion geometry, Paul[3] derived a direct expression for Young's modulus. If the inclusions are taken as porosity his relation reduces to

$$\frac{E}{E_o} = \frac{1 - P^{2/3}}{1 + P - P^{2/3}} \qquad 2\text{-}4$$

This expression assumes Poisson's Ratio of the porosity to be equal to that of the solid and is therefore questionable.

Hashin[4] has dealt with the problem of spherical pores and obtained a closed expression for bulk modulus and upper and lower bounds for shear modulus. The effective bulk modulus of the porous body is given by

$$\frac{K}{K_o} = 1 - \frac{3(1-\nu)P}{2(1-2\nu) + (1+\nu)P} \qquad 2\text{-}5$$

where ν is Poisson's Ratio of the solid.

The upper and lower bounds of the shear modulus of a porous body with arbitrary pore shape is given by

$$1 - \frac{15(1-\nu)P}{(7-5\nu) + \left[2(4-5\nu) - \frac{126}{7+5\nu}\phi(P)\right]P} \leq \frac{G}{G_o} \leq 1 - \frac{15(1-\nu)P}{7-5\nu_o + 2(4-5\nu_o)P}$$

2-6

where

$$\phi(P) = \frac{(1-P^{2/3})^2}{1-P^{2/3}}$$

Generally, the above theoretical relationships predict values which are 10 to 20% higher than measured values. Buch and Goldschmidt [5] have stated that it is impossible to apply the theoretical formulas to sintered bodies on the basis of the elastic moduli of the fused material. Their explanation for the divergence between theory and experiment with increasing porosity was based on the "diminished elastic properties of grain boundaries." This interpretation would necessarily imply a grain size effect on the elastic properties of fully dense polycrystalline materials. To date no investigation has demonstrated an effect of grain size (or more precisely the effect of amount and condition of grain boundaries) on elastic properties.

Although the explanation by Buch and Goldschmidt was given in reference to the condition of the grain boundaries (apparently referring to the grain boundary thickness and degree of crystallographic disorder) a comparison of Young's modulus calculated from single crystal data and measured values on fully dense polycrystalline material should indicate the validity of their reasoning. This comparison has been made by Wachtman et al. [6] for corundum. Their work produced calculated lower and upper bounds for Young's modulus of 57.6 and 59.2 x 10^6 psi, respectively. Measured values [7,8] for

polycrystalline corundum commonly fall in the range of 57.8 to 58.1×10^6 psi in very good agreement with the single crystal data.

In order to quantitatively summarize experimental data a number of empirical or semi-empirical relations have been proposed. Three of the most commonly used equations are listed below:

$$M = M_o e^{-bP} \qquad 2\text{-}7$$

$$M = M_o(1-\alpha P) \qquad 2\text{-}8$$

$$M = M_o \left[1 - \frac{AP}{1+(A-1)P}\right] \qquad 2\text{-}9$$

where: M can be the shear modulus (G) or Young's Modulus E

M_o is the modulus at zero porosity

P is volume fraction porosity

b, α and A are empirically determined constants

It has become common practice to statistically determine which of the above general equations best fits any given set of experimental data.

Equation (2-7) was proposed by Spriggs[9] and has been shown to fit data for Al_2O_3 and MgO to porosity values greater than 25%. The exponential relation would not be expected to be adequate for values of porosity greater than 40%. This is obvious from the fact that the equation does not predict zero moduli values at 100% porosity.

The linear form of Equation (2-8) has been found to adequately describe the dependence of elastic moduli on porosity for a number

of materials.[10,11,12] Equation (2-8) does have some theoretical basis in that it is the general form of Mackenzie's equation for shear modulus when the dependence of Poisson's Ratio on porosity is ignored.

Equation (2-9) was proposed by Hasselman[13] and also has some theoretical basis since it has the same functional dependence on porosity as Hashin's upper bound for the shear modulus.

2-2 Preparation and Characterization of Boron Suboxide

A major portion of the following discussion of boron suboxide is taken from Petrak, Rah and Doosey.[33] The specimens used for their work were the same as those used for the elastic properties study of B_6O.

The boron suboxide phase was reported as early as 1909 by Weintraub[14] who prepared this material by reduction of B_2O_3 and determined the composition to be B_2O by chemical analysis. The existence of B_2O was later questioned in 1926 by Kahlenberg[15] who suggested that B_2O was a mixture of B_2O_3 and B. Almost no mention of this material was found in the literature until Paternak's investigation in 1959.

Boron suboxide is generally characterized as a hard material (measured to be slightly harder than B_4C) with theoretical density of 2.60 gm/cm^3. It is a stoichiometric compound with a stoichiometry of B_6O and a rhombohedral crystal structure. Boron

suboxide will begin to oxidize to B_2O_3 at approximately 500 to 600°C in air and will decompose at temperatures above 1000°C in an inert atmosphere. It is easily prepared by reaction hot pressing of appropriate amounts of B_2O_3 and elemental boron as well as the simple reaction of these components at 1400°C in an inert atmosphere. B_6O has also recently been prepared by heating mixtures of zinc oxide and boron.[16] Preparation by either of the latter methods, however, would be insignificant as a step toward producing a dense body. Because this compound decomposes rapidly above 1500°C at atmospheric pressures, densification by conventional sintering techniques would appear impossible.

The thermal expansion coefficient of boron suboxide was found to increase from 3×10^{-6}/°C near room temperature to 5.7×10^{-6}/°C at 900°C. A room temperature electrical resistivity value of 10^6 ohm-cm indicated a relatively high thermal conductivity compared to most oxide ceramics.

2-2-1 Preparation of Dense Boron Suboxide

The compositions studied were prepared from appropriate mixtures of anhydrous boric acid and amorphouse boron powders.* The anhydrous boric acid powder had a particle size

*U. S. Borax Research, U.S. Borax and Chemical Corporation, Anaheim, California

range from approximately 0.01 to 1 mm, while the amorphous boron powder was from 0.01 to 4.0 μm. Figure 2-1 shows photomicrographs of both powders. Emission spectrographic analyses revealed an impurity level of less than 0.1% for the boric acid and approximately 1% for the boron exclusive of boric oxide. The boron powder was known to contain approximately 4% boric oxide, of course this was not considered an impurity. A list of impurities is given in Table 2-1.

The hot pressing of specimens in this study was accomplished in two steps. The first was a prepressing operation which consisted of heating the dry mixed starting powders in a steel die to approximately 500°C at 3 ksi for 5 minutes. Under these conditions the anhydrous boric acid was molten. A nichrome wire heating element and bench top press were used during the prepressing step. The steel die was first lined with pyrolytic graphite sheet * and then 0.005 in. tantalum sheet before inserting the powder mixture. The pyrolytic graphite facilitated easy removal of the specimen from the die while the tantalum assured smooth specimen surfaces. The purpose of the prepressing operation was (1) to consolidate the compact and impart green strength as well as (2) to disperse the anhydrous boric acid. Examination of fractured surfaces of a prepressed specimen revealed maximum boric acid agglomerate size of approximately 100 μm.

* Grafoil-Union Carbide Corporation

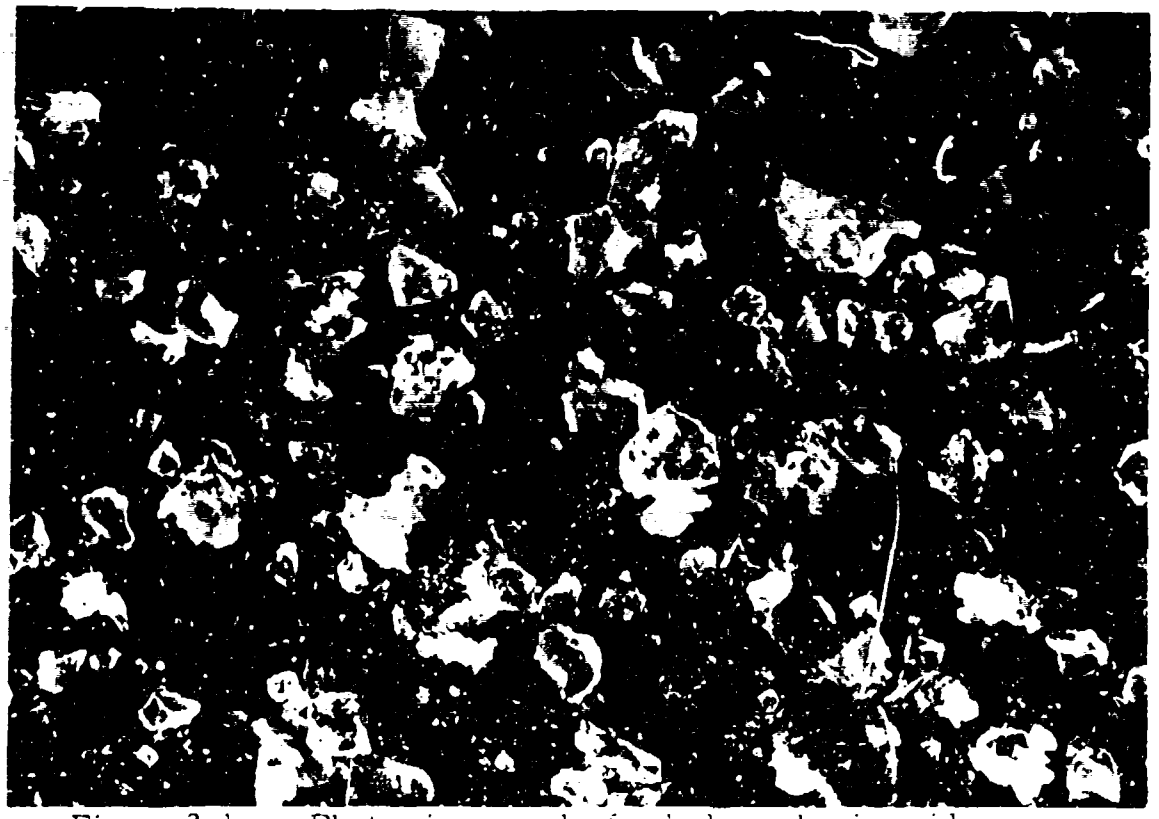

Figure 2-1 a. Photomicrograph of anhydrous boric acid. (10, 75X)

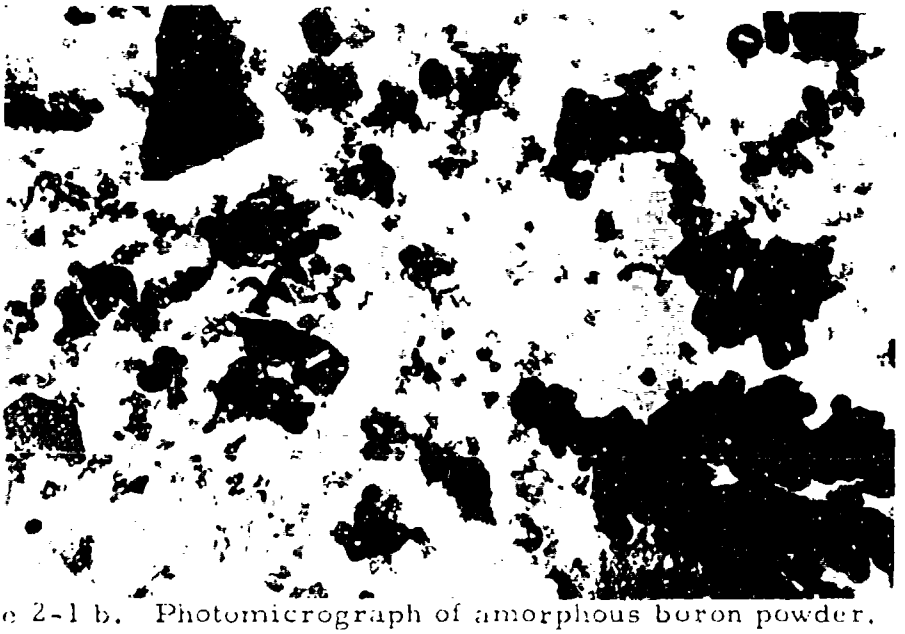

Figure 2-1 b. Photomicrograph of amorphous boron powder. (30, 000X)

Table 2-1 List of Impurities for the Starting Materials and a Typical 80 wt % Boron Composition Hot Pressed at 1950°C. Determined by Emission Spectrographic Analyses

Impurity	Boron	Anhydrous Boric Acid	Boron Suboxide
	ppm	ppm	ppm
Mg	5000	3	2000
Al	1000	100	900
Si	800	50	500
Mn	300	< 30	400
Fe	300	150	300
Ca	300	< 30	300
Cr	80	< 30	60
Ni	80	< 30	90
Cu	80	< 10	60
Pb	< 30	< 30	< 30
Ag	< 3	< 3	< 3
Mo, Zr, Sn	< 30	< 30	< 30
Nb, Ti	< 100	< 100	< 100
W, Cd	< 300	< 300	< 300

The second step was a more conventional hot pressing operation. This was accomplished in vacuum using inductively heated ATJ* grade graphite dies with barrier layers of boron nitride and tantalum. A schematic diagram of the furnace and die assembly is shown in Figure 2-2. The boron nitride** was applied to the grooved cylindrical surfaces of the die and punches using a suspension in toluene. (Dipping the punches in the suspension and a simple slip casting method in the die gave very uniform layers of boron nitride.) Initial pressings without the tantalum barrier revealed a ring of boron carbide 3 to 5 mm thick on the circumference of the specimen. The use of tantalum prevented any significant formation of boron carbide, and tantalum was not found to diffuse significantly into the billet. X-Ray diffraction analysis of the tantalum barrier after a typical pressing showed tantalum carbide as the main phase with smaller amounts of TaB_2 and Ta metal. As an added precaution, however, the outer 3 mm of each specimen were always discarded before any tests were performed.

A billet size of 5 cm in diameter by 1.2 cm in thickness was used so that adequate material was available for many different analyses and tests. Pressings were made at 1900 to 2000°C for 15

*Union Carbide Corporation

**High Purity Fine Grade - Carborundum Co.

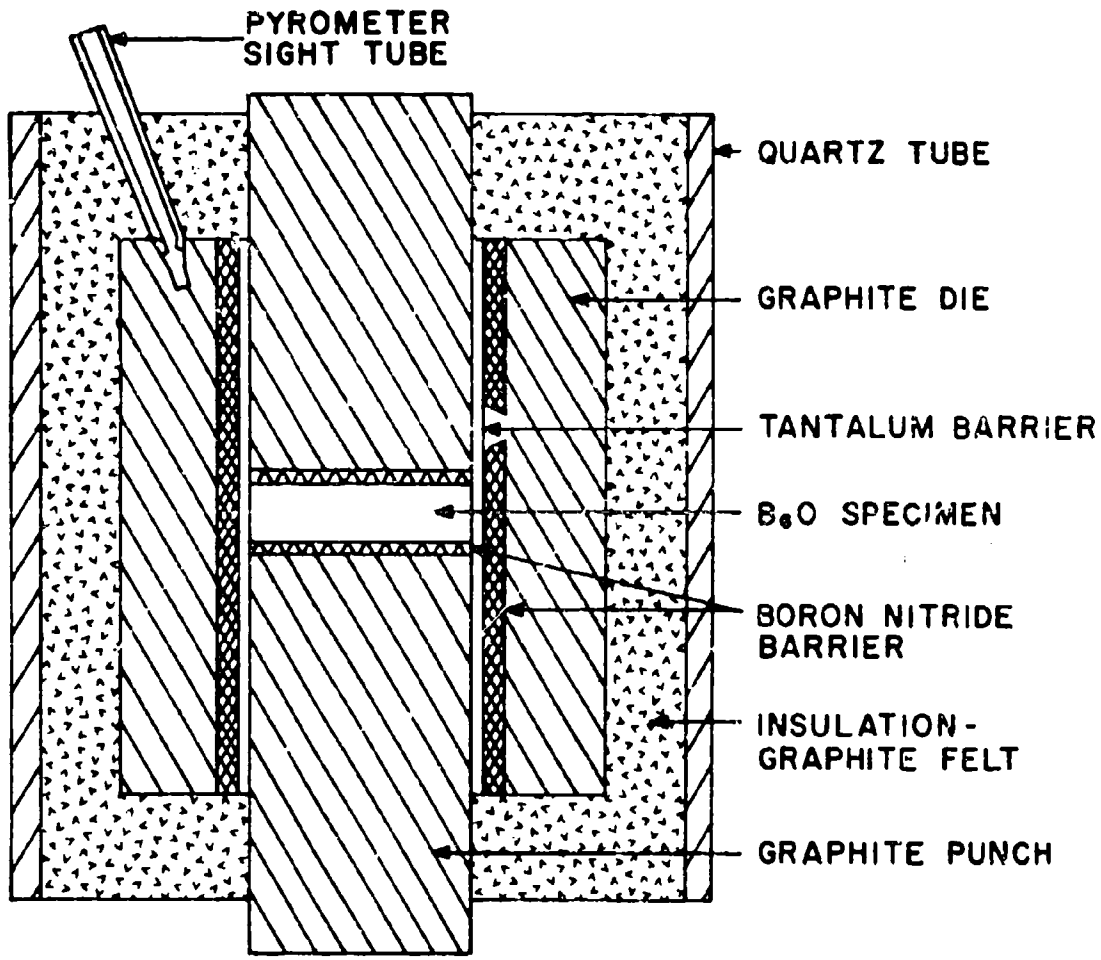

Figure 2-2. Furnace and die assembly for hot pressing boron suboxide

to 30 minutes at 6 ksi. Densification was monitored by means of a dial gauge mounted on the press ram. Densification due to sintering was not observed until the 1750 to 1800°C temperature range was attained. Pressure was maintained at 0.5 ksi up to the sintering temperature and then increased to 6 ksi. The heating rate from room temperature to 1100°C was relatively high at approximately 80°C/min, and then reduced to approximately 20°C/min up to 1500°C. Higher heating rates from 1100 to 1500°C tended to produce cracked billets. This is probably due to the fact that the B_6O phase begins to form at approximately 1100°C and is not complete until about 1500°C under heat up conditions. These pressing parameters were found to work equally well for compositions in the 80-100 atomic percent boron range and bulk densities greater than 99% of theoretical were obtained.

2-2-2 Microstructure and Microhardness

Polished specimens were prepared for metallographic examination by mounting a chip of hot pressed material in thermo setting plastic and grinding and polishing with diamond. Diamond impregnated resin wheels from 180 grit to 2000 grit and in some cases 1, 0.5 and 0.1 μm diamond paste were used for the surface preparation. As will be discussed later, compositions with a boron content less than 80 wt % would necessarily contain B_2O_3 which is readily soluble in H_2O. Because H_2O was used as a coolant during

grinding, pull outs were always experienced in specimens containing B_2O_3 and representative surfaces nearly impossible to obtain. Representative surfaces for compositions containing greater than 80 wt % boron on the other hand were relatively easy to obtain using diamond preparation media.

Figure 2-3 shows a 78% boron composition. The lighter phase is boron suboxide and the dark phase is porosity and pullouts. The measured bulk density of this specimen was 2.54 gm/cm^3 (2.60 gm/cm^3 accepted as theoretical for B_6O). Since the density of B_2O_3 is approximately 1.8 gm/cm^3 and approximately 4% of B_2O_3 was known to be present, the specimen was actually 98.8% of theoretical density. Figure 2-4 shows an 85% boron specimen. The light phase in this photomicrograph is boron and the dark phase is boron suboxide. As can be seen very little porosity is present. In compositions containing more than 5 to 10% free boron, the boron phase is well distributed, whereas an agglomerated threadlike distribution was often observed in specimens containing small amounts of free boron.

High density boron suboxide was prepared with very little grain growth from the starting boron powder. Figure 2-5 shows a 99% dense, 80% boron composition with an average grain size of 1 μm. However, by hot pressing at higher temperature ($\geq$ 2000°C) for times longer than 30 minutes, secondary grain growth was observed as is shown in Figure 2-6. This exaggerated grain growth

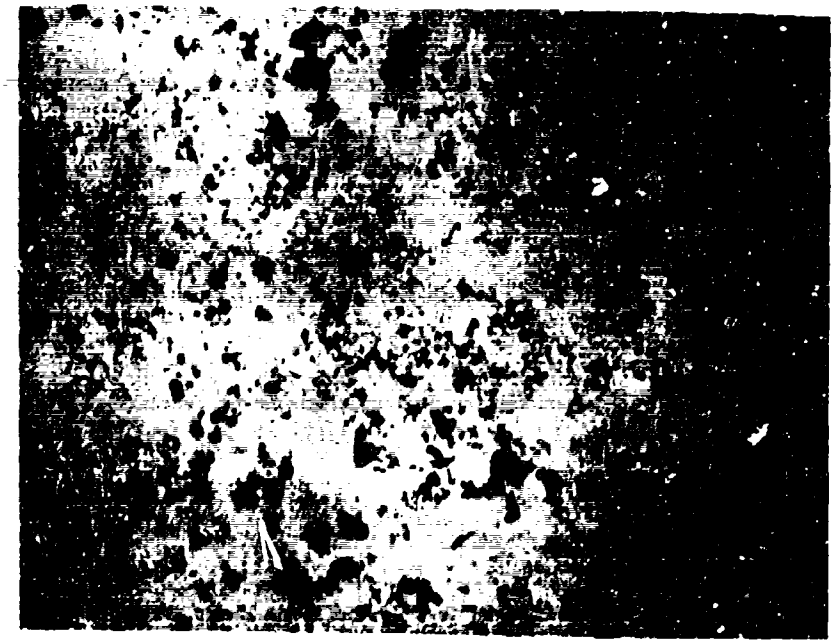

Figure 2-3. Photomicrograph of a 78 wt % boron specimen. (200X)

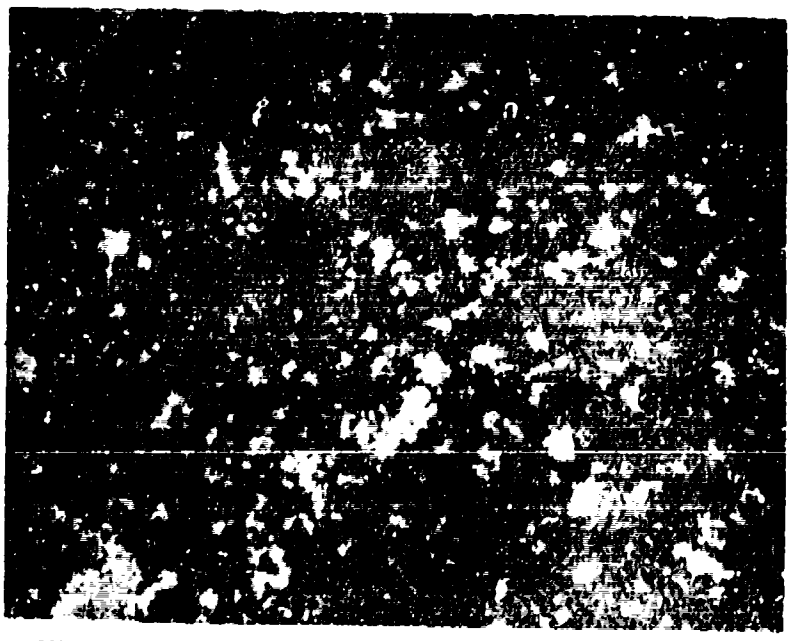

Figure 2-4. Photomicrograph of an 85 wt % boron specimen. (600X)

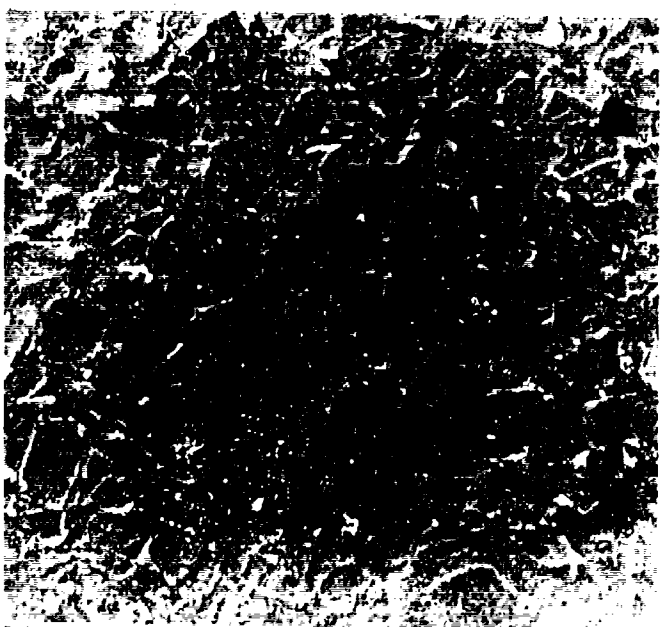

Figure 2-5. Electron micrograph of a 99% dense 80 wt % boron specimen. (Replication of a fractured and etched surface. 10,000X)

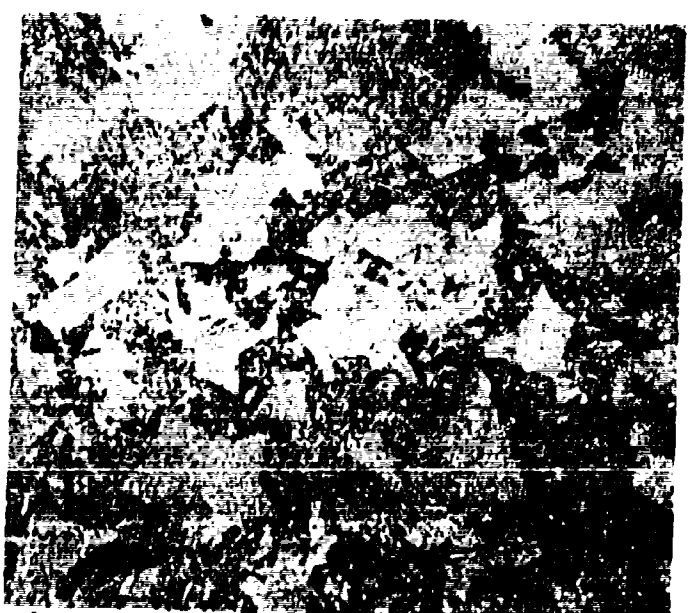

Figure 2-6. Photomicrograph showing secondary grain growth of boron suboxide. (250X)

was probably affected by the relatively wide particle size distribution of the starting boron powder.

The microhardness of boron suboxide was found to be slightly higher than that of boron carbide when specimens of each material were tested at the same time by the same operator using the same equipment. The average hardness values were 3042±150 kg/mm^2 for boron suboxide and 3015±130 kg/mm^2 for boron carbide. These values represent averages of 22 indentations for boron suboxide and 16 indentations for boron carbide. All measurements were made with a 100 g load using a Wilson Tukon Hardness Tester and a Knoop diamond indenter.

2-2-3 Crystal Structure and Stoichiometry

Boron suboxide reflection data were first indexed on an orthorhombic unit cell by Pasternak [17] who also determined the composition to be $B_{6.6}O$ by chemical analysis and the measured density to be 2.64 gm/cm^3. Based on these data he assigned a stoichiometric formula of B_7O. Later, La Placa and Post [18] showed that the powder pattern for the boron suboxide phase could be more satisfactorily indexed on the rhombohedral cell of the boron carbide structure type. It has been pointed out by Post [19] that the ambiguity in indexing the pattern was the result of a special intensity ratio which exists; namely $[d_{(001)}/d_{(100)}]^2 = 7$. La Placa and Post suggested a $B_{13}O_2$ stoichiometry which agreed well with Pasternak's $B_{6.6}O$ composition

but required a calculated density of 2.80 gm/cm^3. Rizzo et al.[20] found the composition to be B_6O which was later supported by Post.[19] A $B_{12}O_2$ structural formula together with the hexagonal lattice parameters of a = 5.395 and c = 12.342 Å as determined by Rizzo et al, gave a calculated density of 2.59 gm/cm^3.

The proposed $B_{12}O_2$ structure ($R\bar{3}m$ space group) is shown in Figure 2-7. It is similar to the B_4C structure in that boron icosahedra form the rhombohedral frame work of the unit cell.[21] Boron carbide (B_4C) though has three carbon atoms along the c-axis; two in the 2c position and one in the 1b position. The 1b position can, however, be occupied by a boron atom, thus giving a $B_{13}C_2$ structural formula. Boron carbide is generall accepted to exist over a composition range from B_4C to $B_{13}C_2$[22,23], though it has been reported to exist from 79 to 96[24] atomic percent boron. Assuming this rhombohedral symmetry, Hoard and Hugi s[23] have noted that the only dimensionally satisfactory structure that satisfies the Longuet-Higgins and Roberts electron counting rule[25] for a filled band configuration is $B_{12}O_2$ where no bond exists between oxygens. This would rule out any stoichiometry range for boron suboxide analogous to the B_4C-$B_{13}C_2$ range in boron carbide.

Although no single crystal structure analysis has as yet been complete[d], [the] work of [illegible][26] on powder patterns and Corfield[27] on twinned [illegible] the $P\bar{3}1m$ space group for

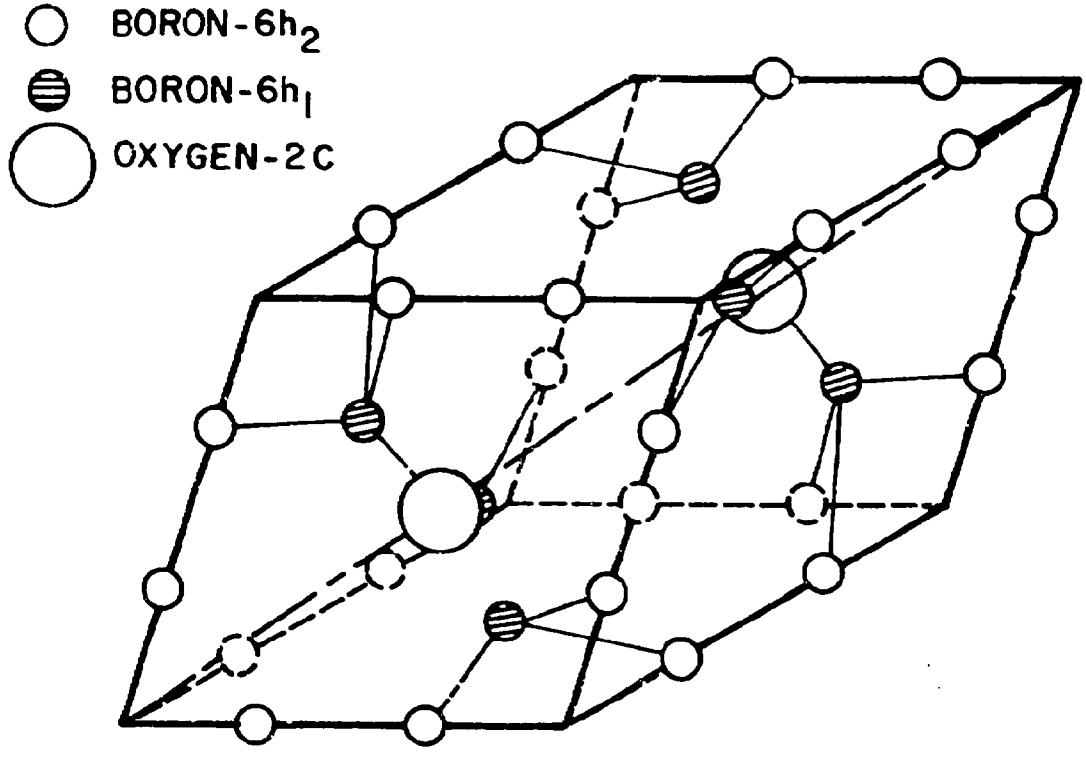

Figure 2-7. Proposed $B_{12}O_2$ structure for boron suboxide.
(Modified from reference 21)

boron suboxide. A lattice parameter and pycnometric density study was accomplished, however, in order to determine whether a stoichiometry range does exist for boron suboxide.

Precision lattice parameters were determined at room temperature on hot-pressed specimens with nominal starting compositions of B_4O, B_5O, B_6O, B_7O and B_8O. Two different methods were used for determining peak positions, namely (1) slow scan diffractometer traces and (2) Debye-Scherrer film techniques using a camera with a radius of 71.62 mm. Agreement between the two methods was very good. However, the film technique yielded the more precise results, and these results are given. The method used for the computation of lattice parameters was the same as that used in Reference 28. As is shown in Table 2-2, the hexagonal lattice parameters for all five specimens were within the range of a = 5.385±0.003 and c = 12.325± 0.005 Å, thus indicating no significant change. Furthermore, observable amounts of B_2O_3 were noted in the B_4O and B_5O specimens by X-ray diffraction, while free boron was found in the B_7O and B_8O specimens. The free boron in the B_7O specimen could not be detected by X-ray diffraction but was observed by metallographic analysis.

Chemical analyses * are also shown in Table 2-2. The nominal B_6O and B_7O specimens contained 79.7 and 80.7 wt % boron which

---

* Performed by Ledoux and Company, Teaneck, New Jersey.

Table 2-2 Lattice Parameters, Phases Present and Pycnometric Density of Various Boron Oxygen Compositions

Nominal Composition	Analyzed Composition Wt % B	Hexagonal Lattice Parameters a(Å)	c(Å)	Phases Present	Density gm/cm^3
B_4O	79.0	5.387±0.002	12.323±0.004	B_2O_3 + boron suboxide	2.601
B_5O	77.5	5.384±0.002	12.330±0.005	B_2O_3 + boron suboxide	2.600
B_6O	79.7	5.386±0.001	12.327±0.003	Boron suboxide	2.593
B_7O	80.7	5.388±0.002	12.325±0.003	Boron suboxide + rhombohedral boron	2.607
B_8O	82.5	5.382±0.002	12.323±0.003	Boron suboxide + rhombohedral boron	-

supports a B_6O stoichiometry (80.2 wt % boron) for the suboxide phase. Chemical analyses were performed for both boron and oxygen. The boron contents were determined by wet chemical techniques and are considered more accurate. Oxygen analyses were obtained by inert gas fusion. The totals for boron and oxygen content were between 99.0 and 100.4 wt %. These values were not unreasonable since typical impurity values totaled 0.6 wt %.

Pycnometric densities were also determined on all but the B_8O specimen. At least 5 grams of each composition was ground to pass a 325 mesh sieve in a boron carbide mortar and pestle, then boiled in distilled H_2O to dissolve any B_2O_3 present. After filtering and drying the density was measured using a 25 cm^3 pycnometer with butyl alcohol. In each case the pycnometer containing powder and butyl alcohol was heated to the boiling point of the alcohol for 1 hour then cooled and evacuated for 1 hour. All weighings were made at 24±0.3°C. This method was found to give the most precise results.

All density values were within the range 2.600±0.007 gm/cm^3 as is shown in Table 2-2. This average value agrees well with a calculated value of 2.602 gm/cm^3 obtained by assuming a B_6O stoichiometry and the average lattice constants found in this study. Further, assuming the average lattice parameters found here, the B_4O and $B_{13}O_2$ stoichiometries would require densities of 2.87 and 2.78 gm/cm^3, respectively. Thus all of the above data support the

$B_{12}O_2$ structural formula in agreement with the Longuet-Higgins and Roberts theory.

Polished specimens of the nominal compositions mentioned previously were studied by Baun and Solomon [29] using a Perkin-Elmer (Hitachi) XMA-5 electron microbeam probe. Typical oxygen K spectra for boron suboxide and B_2O_3 are given in Figure 2-8. It is seen that B_6O showed two maxima separated by approximately 3 eV, while B_2O_3 had a major peak with a much weaker component at the low energy side.

The existence of the two peaks indicates the formation of split molecular orbitals. Although a complete molecular orbital treatment was not performed for B_6O the two transitions could be explained by the crossover theory. On this basis, transitions from the boron 2 p to the oxygen 1 s level as well as the oxygen 2 p to 1 s are allowed. Using published values for these energy levels, the two bonds should be 2.5 to 3 eV apart as was observed.

Baun and Solomon, in comparing the spectra from the nominal compositions, have noted changes in the relative intensities of the two peaks. They have explained these changes on the basis of compositional changes due to different combinations of boron and/or oxygen occupying the interstitial 2 c or 1 b sites in the rhombohedral structure of Figure 2-7. Experimental evidence as well as theoretical considerations disagree with this explanation. Alternatively, since

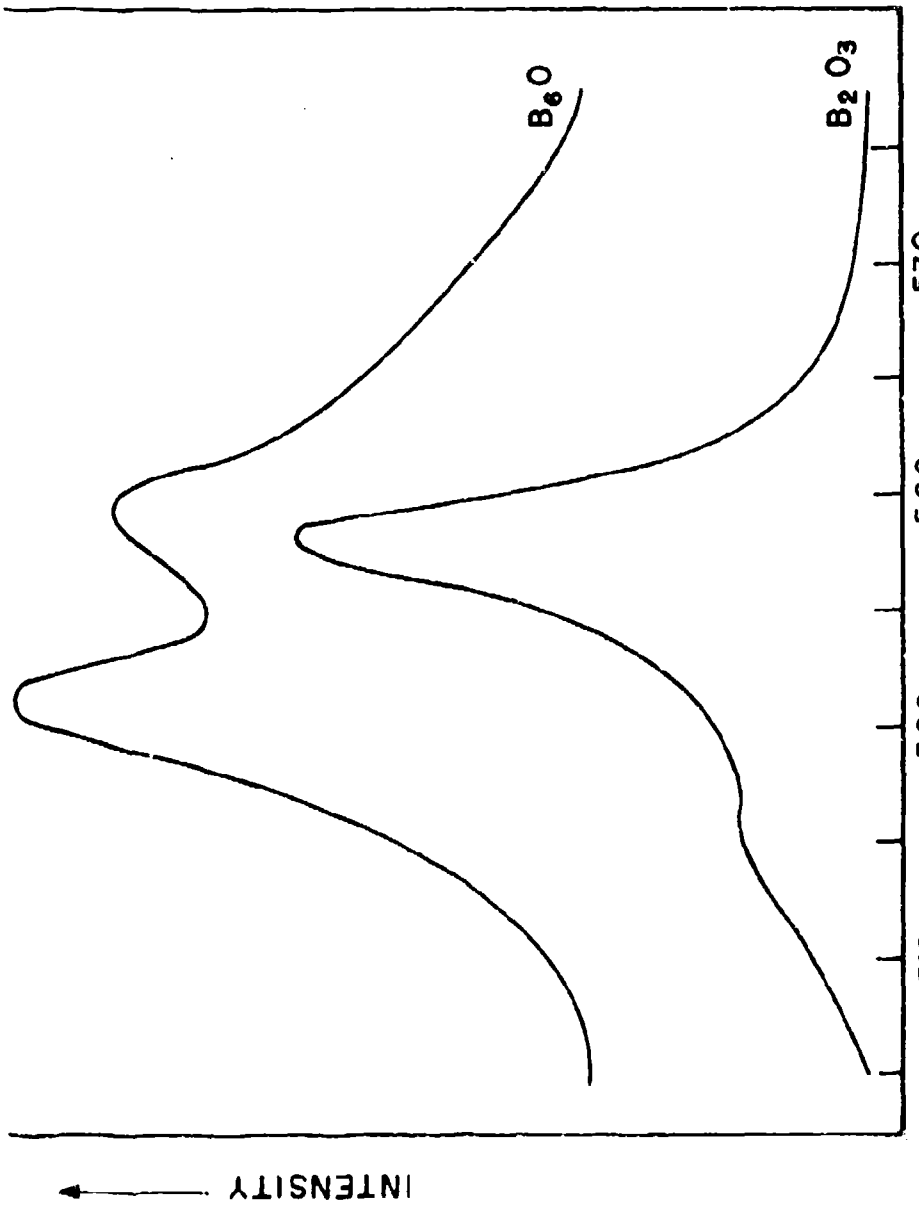

Figure 2-8. Oxygen K emission spectra for boron suboxide and B_2O_3

some of the specimens studied were known to contain a second phase of B_2O_3, the observed changes could be due to the super position of the two spectra shown in Figure 2-8. This explanation is further substantiated by the fact that changes in observed spectra were noted from different areas in the same specimen. Any small amount of B_2O_3 present would necessarily be located at the B_6O grain boundaries. Specimens, in which secondary grain growth had occurred, gave spectra indicating a higher boron content when only single large grains were analyzed and lower boron content when many small grains were analyzed together.

The infrared reflection spectrum for the B_6O phase has been determined by Phillipi.[30] The main reflection band at 1060 wave numbers is shown in Figure 2-9. Other weaker bands were observed at 880, 780, 710, and 420 wave numbers. Similar reflection spectra were observed for the nominal compositions of B_4O, B_5O, B_6O and B_7O. However, no significant changes in the spectra that could be related to changes in stoichiometry were evident.

2-2-4 Stability and Mass Spectrometric Studies

The stability of boron suboxide was investigated as a function of temperature in a flowing helium atmosphere. A 97% dense hot pressed pellet was repeatedly heated to temperature, held for two hours, cooled and weighed. Results are presented in Figure 2-10. After the final heating cycle the specimen had an

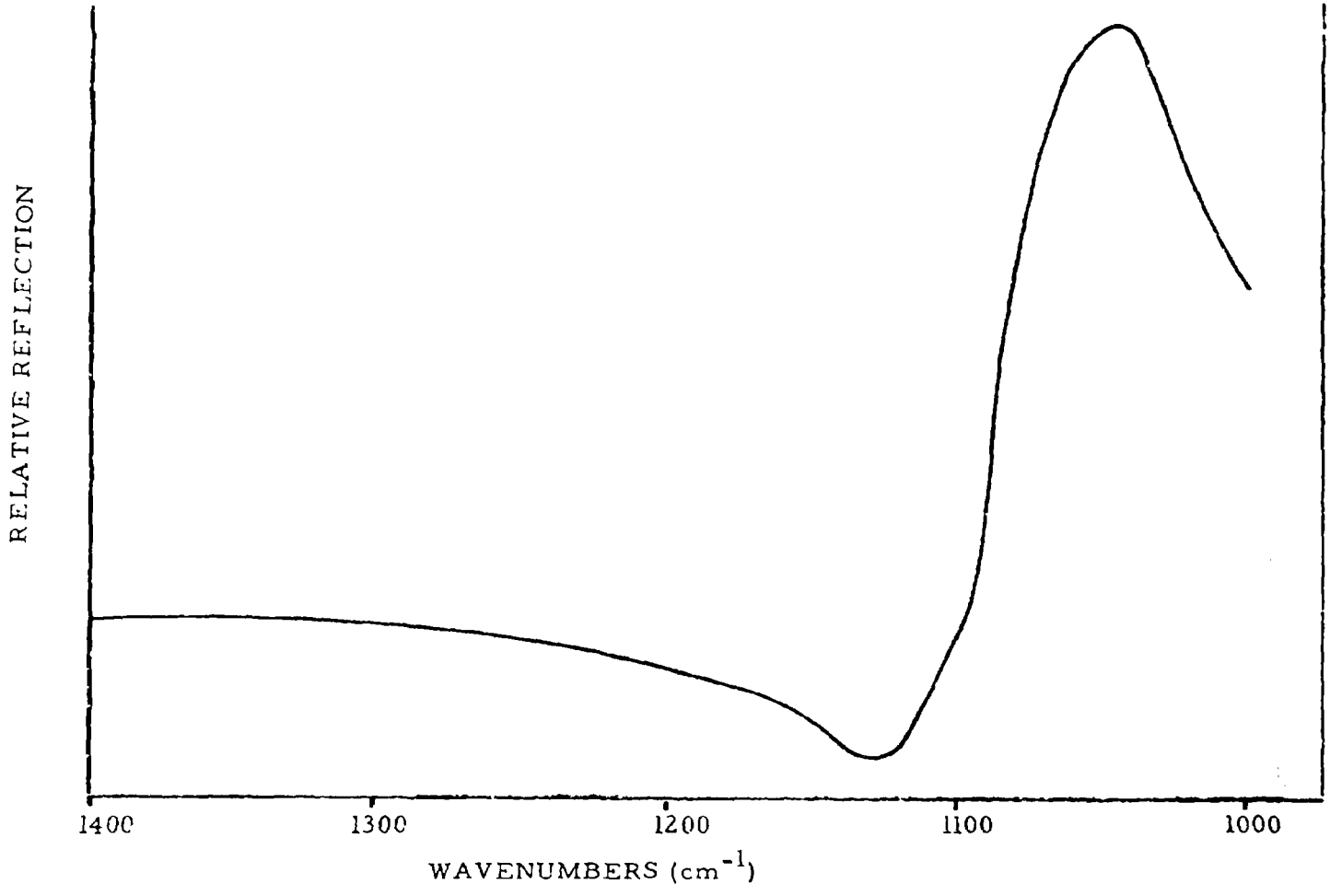

Figure 2-9. The main infrared reflection band observed for boron suboxide

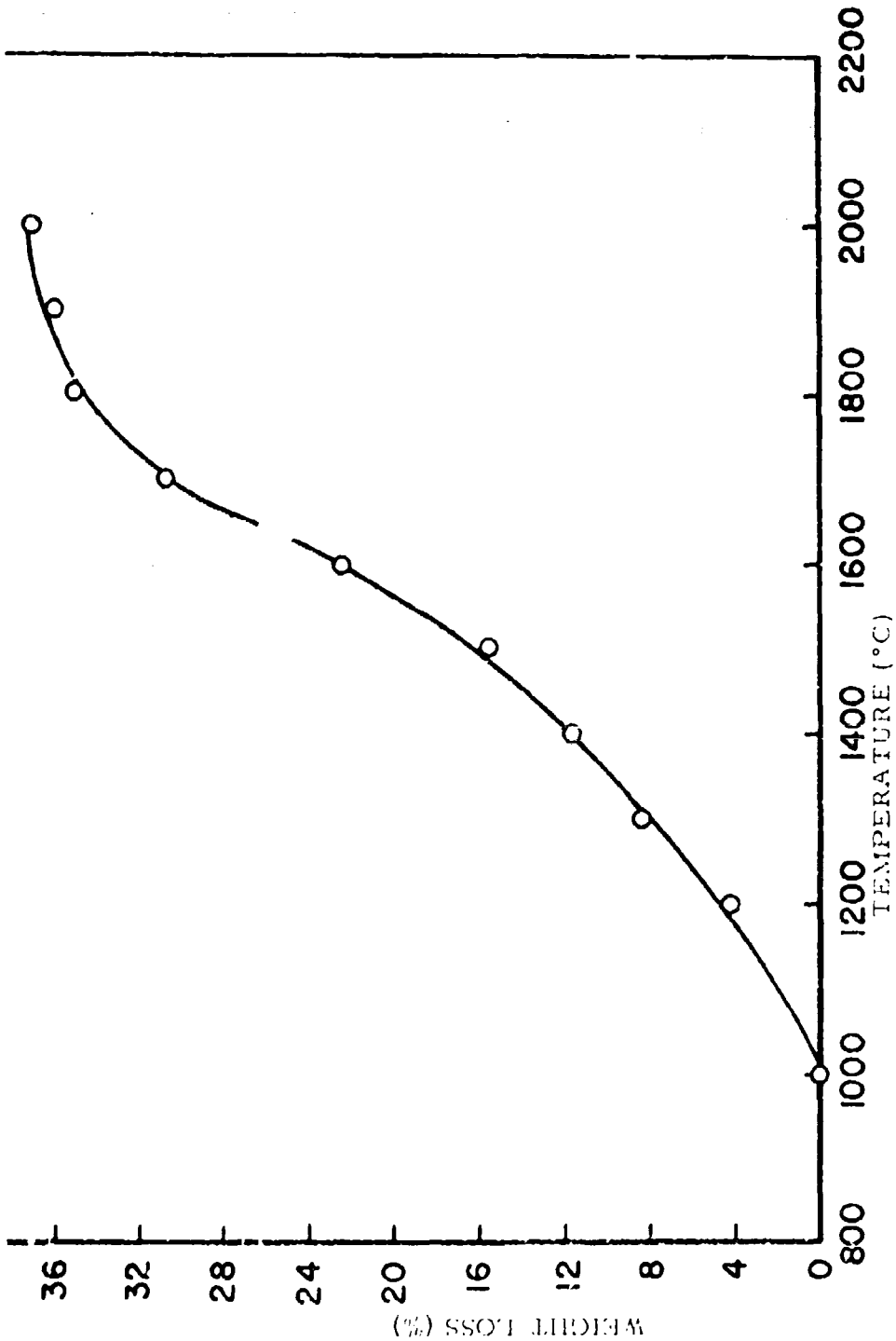

Figure 2-10. Weight loss curve for a 97% dense boron suboxide specimen heated in a flowing helium atmosphere

extremely porous appearance and could be crushed easily. X-Ray diffraction analysis of the decomposed material revealed rhombohedral boron and a small amount of boron suboxide. This would explain the decrease in rate of weight loss at the higher temperatures, since most of the boron suboxide had already been decomposed. This work is in reasonable agreement with that of Rizzo et al.[20] who determined weight loss in helium for the 1300-1750°C temperature range.

The vaporization characteristics of boron suboxide were investigated by Carbonara and Alexander[31] to determine the vapor species and the thermodynamic quantities involved. An analyzed 79.7% boron composition was contained in a BeO lined niobium Knudsen cell. A Nuclide HT-90-12 mass spectrometer was used to identify the vaporizing species to temperatures as high as 2000°C. The predominate vapor components were BO and B_2O_2. Small amounts of B, B_2O, BO_2 and B_2O_3 were also found. This information was used to confirm thermal gravimetric analysis made in an Ainsworth microbalance and the BeO lined niobium Knudsen cell.

The TGA data were converted to equilibrium total pressure and ΔH_v and ΔS_v were calculated for the reaction:

$$2B_6O(s) \rightleftharpoons B_2O_2(g) + 10B(s)$$

$$\Delta H_v = 90.9 \text{ kcal/mol}$$

$$\Delta S_v = 40.2 \text{ eu}$$

X-Ray diffraction analysis on the condensed phases afte testing gave both boron suboxide and rhombohedral boron. No reaction with BeO was detected.

The above values for ΔH_v and ΔS_v compare well with ΔH_v = 94±8 kcal/mol and ΔS_v = 41.4 eu found by Inghram et al.[32] for the vaporization of mixtures of boron and boric oxide. Their work was done in the temperature range 1030 to 1230°C on molar ratio of boron to boric oxide greater than one. Since Inghram et al. reported no analysis on their condensed phases an attempt was made to reproduce them. A 2:1 molar ratio of boron to boric oxide was mixed and placed in a covered alumina crucible (Inghram et al. used an alumina Knudsen cell). The crucible was then heated to 1230°C in vacuum for 7 hours. The condensed phases under these conditions were found to be B_2O_3 and B_6O with only a small indication for boron. It is suggested that Inghram et al. actually observed the vaporization of B_6O and B_2O_3. This would explain the similarities in the results of the two mass spectrometric studies.

2-3 Diametrical Compression of a Sphere

Although the stress distribution in a diametrically loaded sphere is not available in any of the standard texts on elasticity the problem has been analyzed by Shook.[34] His solution, presented in Appendix B, considers the effect of load distribution and Poisson's ratio.

Hiramatsu and Oka[35] have also considered the problem in regard to the diametrical compression of irregularly shaped rock specimens. They provided a mathematical analysis of the problem for spherical specimens giving the following approximate equation for maximum tensile stress:

$$\sigma = 0.9\, P/d^2 \qquad 2\text{-}10$$

where: P is applied load and d is the sphere diameter.

Their equation is proposed to be applicable for the following conditions:

loaded diameter/sphere diameter < 0.083
Poisson's Ratio in the range 0.14 to 0.33

A comparison of their analysis with that of Shook (see Figure B-2) shows excellent agreement for loaded diameter/sphere diameter equal to 0.083 and Poisson's ratio of 0.30. Shook's analysis, however, predicts a value of 1.5 for the constant in equation (2-10) at Poisson's ratio of 0.15. At a loaded diameter to sphere diameter ratio of 0.04, for example, Shook gives values from 1.9 to 4.7 depending on Poisson's ratio.

Hiramatsu and Oka also performed photoelastic studies on spherical and irregular geometries to demonstrate the presence of tensile stresses along the loaded axis of the specimens. The observed stress distributions closely resembled the well documented[43] stress distribution in a diametrically loaded cylinder.

3. Mode of Investigation

Before attempting to apply the analysis provided by Shook, it was decided to substantiate experimentally that fracture initiation would occur in the region of maximum tensile stress. This was accomplished by photographing the failure of glass spheres. High speed moving film techniques were employed at first. Because this method proved unsuccessful, single photographs were taken using a camera with an open shutter in a darkened room. The interruption of a beam of light by the initiation of fracture in the glass sphere provided a signal to a flash light source. This technique was found to be satisfactory.

As supporting evidence that fracture was not initiated at a point on the surface, the tensile strengths of glass spheres with varying degrees of surface finish were determined. Observed strength values can usually be related to the size of defects at the point of fracture in brittle materials. If fracture was initiated at the surface (this is thought to be the case in all other methods of testing tensile strength of brittle materials), then the expected strength values would be lower for specimens with rough surfaces than for specimens with polished surfaces.

In order to obtain distributed loads rather than near point loading, metal plates were used as padding materials. The hardness and thickness of the metal pads had to be matched to each specimen size

and estimated strength in order to obtain the desired load distribution. The permanently deformed pads provided a record of the loaded area of the sphere.

The plan of investigation also included the determination of the effect of porosity on the elastic moduli of polycrystalline boron suboxide. These measurements were accomplished using the resonant sphere technique. Since the elastic properties determination required spherical specimens, the boron suboxide spheres were also tested for tensile strength.

4. Materials and Equipment

Descriptions of the materials used in this investigation are listed below:

1) Spherical specimens of boron suboxide were prepared from hot pressed billets. A detailed discussion of the preparation and known properties of these materials is given in Section 2-2.

2) Boron carbide spheres were prepared from high purity hot pressed B_4C obtained from Norton Co., Cambridge, Massachusetts. It had an average grain size of 5 μm and 100 gm Knoop microhardness value of 3015 ± 130 kg/mm^2.

3) The diamond abrasives used in the preparation of B_6O and B_4C spheres were 45, 8 and 1 μm diamond paste obtained from Buehler Ltd., Evanston, Illinois.

4) Polished 3/8 inch borosilicate glass spheres, designated Boro-8330, production lot 31001, were obtained from the Hartford-Universal Co., Hartford, Connecticut. Measured elastic moduli by the resonant sphere technique were $E = 9.0 \times 10^6$ psi, $\nu = 0.195$. The bulk density of the glass was 2.223 gm/cm^3 and the index of refraction was 1.56.

The following is a list of equipment used in this investigation:

1) Appendix A includes a description of the equipment required by the resonant sphere technique for elastic properties determination.

2) Items of equipment used to obtain photographs of diametrically compressed glass spheres were:

a) Fastax-16 mm high speed camera manufactured by Revere-Wollensak Division of the Minnesota Mining Corporation, Rochester, New York

b) Crown Graphic Graflex camera with a 135 mm lens set at f/4.7

c) Photomultiplier -931 A thyratron tube

d) Beckman and Whitley spark gap light source, Model No. 5401, with a 0.3 μsec electrical delay and a flash duration of 150 nano seconds.

e) Edmund Scientific Co. helium-neon laser with a 1 mm beam diameter

f) Dupont High Speed Pan film

g) Carver Laboratory Press, Model B

h) Loading pads were 7075 T6 aluminum

3) A Baldwin-Emery SR-4, Model FGT, testing machine was used for tensile strength measurements of spheres.

5. Experimental Procedure

5-1 Determination of the Elastic Properties of Boron Suboxide

The elastic constants of polycrystalline boron suboxide prepared for this study were determined by the resonant sphere technique. This method was first developed by Fraser and LeCraw [36] and was further evaluated by Schreiber, Anderson and Soga. [37] The actual equipment used for this study was designed by Schreiber et al. under Air Force contract. The reason for its use was that a spherical specimen size of only a few millimeters in diameter was needed as well as the immediate availability of the equipment.

By determining the resonant frequencies of a sphere both the shear velocity of sound and Poisson's Ratio can be determined. This allows the calculation of all the elastic constants of the specimen. The accuracy of this technique is limited only by how accurately the sphere is fabricated. (The spheres prepared for this study were typically within 0.1% of sphericity).

The material requirements for this method are that the specimens be homogeneous and elastically isotropic. This implies the presence of no large cracks and maximum grain sizes << the specimen size. Experimentally, it has been the author's experience that 25% porosity is a maximum for obtaining reliable data. Porosity values greater than 25% effectively reduce the acoustic quality of the specimen such that resonant frequencies can no longer be identified.

Appendix A contains a summary of the theory for the resonant sphere technique and a description of the equipment operation.

5-1-1 Specimen Preparation and Calculations

Two methods of sphere preparation were suggested by Schreiber et al.[37] The first was a pneumatic sphere grinder which randomly abrades a cube into a sphere by forcing it to roll around inside a crucible lined with either a ceramic or diamond impregnated brass. The second method was the contrarotating lapping pipes used by jewelers. Although the second method requires constant attention, it was chosen because it is capable of producing specimens with better sphericity and surface finish. The pneumatic sphere grinder also has the disadvantage of requiring an accurately machined cube in order to obtain a sphere with satisfactory sphericity.

The sphere grinder used in this study is pictured in Figure 5-1. The "pipes or cups" containing the specimen rotate in opposite directions, while the wood dowel rod perpendicular to the direction of the pipes allows the application of side friction. Below the specimen is a dish containing a slurry of abrasive powder and a dispersing fluid. The position of one of the pipes can be adjusted with a thumbscrew. This facilitates specimens of varying size as well as the application of pressure during grinding. The combination of variable pressure on the specimen from three directions along with the opposite rotation of the pipes assures random rotation of the

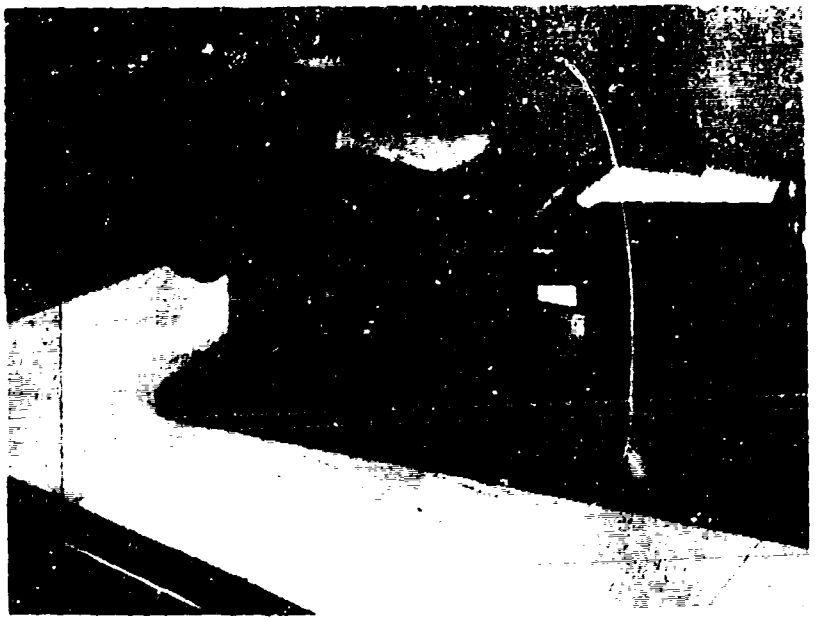

Figure 5-1. Contrarotating pipe apparatus used in the preparation of boron suboxide spheres.

specimen, when given close attention. The random abrasion of the specimen produced a sphere.

The high hardness of B_6O required the use of diamond abrasives in the preparation of spherical specimens. Irregularly shaped pieces of B_6O were first ground by hand, using a coarse diamond wheel, to a more regular polyhedron. The specimens were then ground for approximately 15 minutes using the sphere grinder just described and 80 grit silicon carbide. The coarse silicon carbide was significantly reduced in size after this grinding and accomplished little more than to remove sharp edges and to point out the extremities of the specimen. The extremities were then ground by hand and the silicon carbide grinding repeated. When the specimen appeared to be generally rounded it was ground with 45 μm diamond paste until no flat areas were present. The spheres were then polished using 8 and 1 μm diamond paste.

This procedure took at least 6 hours for each B_6C sphere, although spheres of softer materials such as alumina have been produced in as little as 1 hour. Maximum asphericities of 0.1% were easily obtained for spheres in the size of 0.2 to 0.4 inches. This tolerance though became increasingly difficult to maintain for spheres much smaller than 0.2 inches.

Once a specimen was prepared with sufficient spherical symmetry, the task remained to obtain the acoustical spectrum and to identify each

frequency with a particular mode of vibration. Typically all the vibrational modes between $1T_2$ and $1T_5$ were observed (see Figure A-2 in Appendix A).

Nondimensional frequencies (F_{ND}) were calculated for each observed frequency using the equation

$$F_{ND} = 2.5011 \frac{fi}{fn} \qquad 5\text{-}1$$

where fi is one observed frequency and fn is the observed frequency for the $1T_2$ mode. The edge of a sheet of translucent paper was then superpositioned along the ordinate of an enlarged version of Figure A-2. The calculated nondimensional frequency values were then marked on the edge of the translucent sheet. Sliding the sheet along the abscissa until the marks on the sheet matched the position of the curves provided a graphical determination of Poisson's ratio. The estimated accuracy of this method is ±0.003 for Poisson's ratio.

The shear velocity of sound was then calculated for each observed torsional mode using the equation

$$V_s = \pi d fi/(ka) \qquad 5\text{-}2$$

where: d = sphere diameter

fi = measured frequency

(ka) = theoretical value of the nondimensional frequency taken from Table A-1.

The shear, Young's and bulk moduli were then calculated respectively from the following formulas:

$$G = \rho V_s^2 \qquad 5\text{-}3$$

$$E = 2G(1+\nu) \qquad 5\text{-}4$$

$$K = \frac{EG}{9G-3E} \qquad 5\text{-}5$$

where ρ is the geometrical bulk density of the spherical specimen. Volume fraction of porosity was calculated from

$$P = 1 - \frac{\rho}{2.602} \qquad 5\text{-}6$$

A typical data sheet for one specimen is shown as Table 5-1.

5-2 Photographic Studies of Diametrically Compressed Glass Spheres

A high speed movie camera was used in the first attempt to photograph the fracture of diametrally loaded glass spheres. A maximum frame speed of 32,000 frames per second was used. Lighting was from directly behind the sphere as well as from the sides. The experiments were conducted at ambient atmospheric conditions in the laboratory. Aluminum plates of 1/8 inch thickness were used as contact plates to give a loaded diameter to sphere diameter ratio of 0.30. Because the exposure time for a 200 feet reel of film at 32,000 frames/sec was less than one second, the manual starting of the camera drive had to be coordinated closely with the loading rate of the testing machine. This coordination was

Table 5-1 Typical Elastic Properties Data Sheet for B_6O

Diameter = 0.5793 Mass = 0.2541
Density (ρ) = 2.496 Porosity = 0.041

Resonant Freq (MHz)	Nondimensional Freq	Vibrational Mode	(ka)	Vs Km/sec	$\bar{V}s$ Km/sec
1.1194	2.5011	1T2	2.5011	8.1453	
1.1817	2.6403	1S2			
1.4392	3.2156	2S1			
1.6571	3.7025	1S0			
1.7292	3.8636	1T3	3.8647	8.1430	
1.7361	3.8791	1S3			8.1456
2.0540	4.5893	2S2			
2.2105	4.9391	1S4			
2.2810	5.0965	1T4	5.0946	8.1483	
2.5791	5.7625	2T1	5.7635	8.1439	
2.6579	5.9387	1S5			
2.7493	6.1430	2S3			
2.8051	6.2676	1T5	6.2658	8.1475	

$V_s = \pi df/(ka)$ $\quad G = \rho V_s^2 = 1656$ KBAR $= 24.0 \times 10^6$ psi

$\nu = 0.153$ $\quad E = 2G(1+\nu) = 3819$ KBAR $= 55.4 \times 10^6$ psi

$B = \frac{EG}{9G-3E} = 1835$ KBAR $= 26.6 \times 10^6$ psi

accomplished by slowly loading the sphere to approximately 90% of its expected failure load then rapidly increasing the platen speed and simultaneously starting the camera drive. The success rate for fracturing the specimen during the film exposure was about 75%.

This method of high speed photography proved to be unsuccessful in providing any evidence for the location of fracture initiation. Not only was the maximum frame speed too slow but the glass sphere in a surrounding medium of air acted as a lens with a very short focal length. The light transmitted through the sphere and entering the camera 3 feet away was therefore sharply divergent. The problem of divergent light was dealt with in the next experiment.

In order to get a picture of the location of fracture initiation, a technique was devised to allow the fracture itself to trigger a light source and expose the photograph. The problem of having the glass sphere act as a lens was avoided by containing glycerol around the sphere in a clear plastic cell. Glycerol was used because its index of refraction (n = 1.57) was very close to that of the borosilicate glass spheres. Thus light was permitted to travel through the sphere without being refracted or scattered due to any surface irregularities.

A schematic diagram of this method is shown in Figure 5-2. Because the beam from a laser light source was approximately 1 mm in diameter, the beam was directed through the sphere twice, once slightly above and once slightly below the center of the sphere.

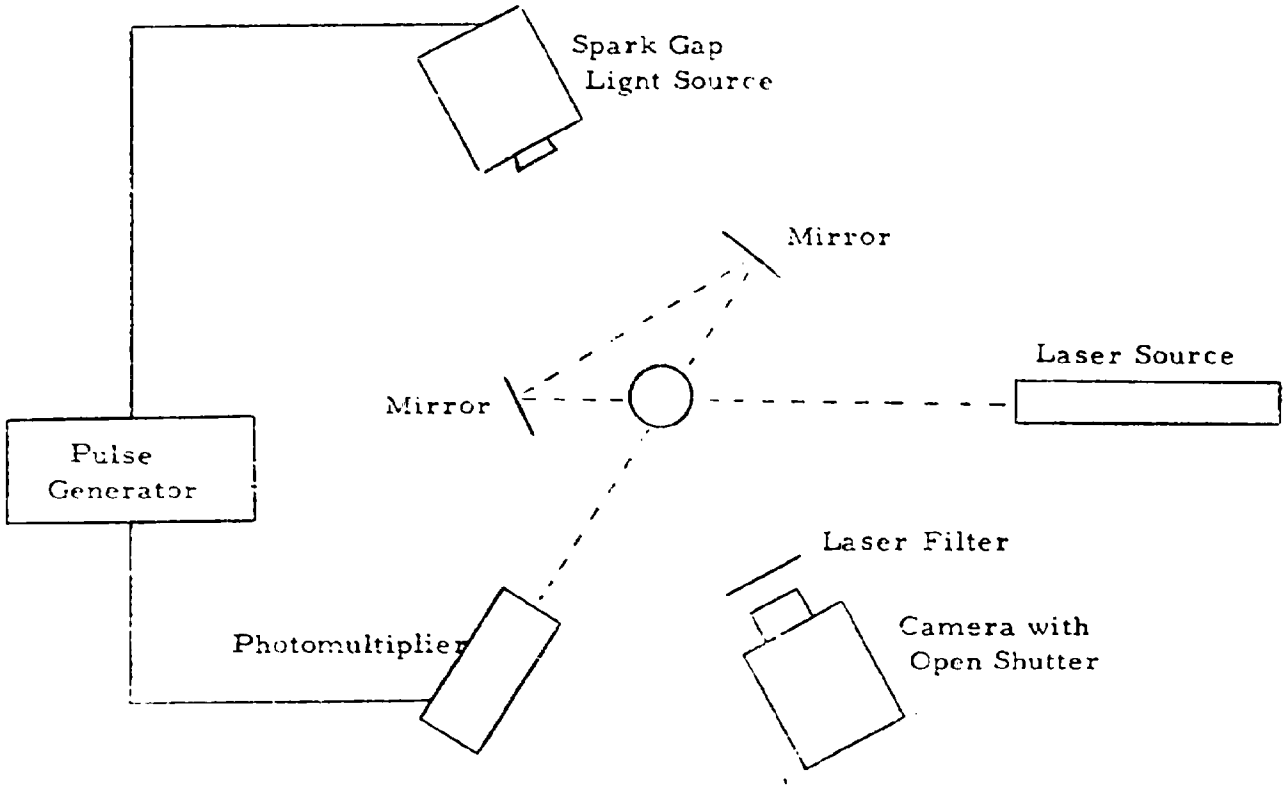

Figure 5-2 Schematic of Experiment to Take High Speed Photographs of a Diametrically Compressed Sphere.

Any interruption of the beam caused by fracture of the specimen would lower the intensity of light entering the photomultiplier. The photomultiplier then gave an electrical signal which triggered a voltage pulse generator which in turn triggered a spark gap light source. Monitoring the signal out of the photomultiplier and out of the pulse generator on a dual trace oscilloscope showed a delay of approximately 2 to 2.5 μ sec. This delay was due primarily to the rise time of the photomultiplier signal. Estimating a maximum 0.5 μ sec delay in the light source, the pictures obtained by this method were taken 2.5 to 3 μ sec after the beam was interrupted. The exposure time of the light source was 0.15 μ sec.

These experiments were done in a darkened room using a camera with an open shutter. A filter was placed in front of the camera to filter the wavelengths of the laser light. Load was applied to the glass spheres using a bench top hydraulic press and 0.25 inch thick aluminum plates were used as pads.

The diametral compression strength of glass spheres with three different surface textures were measured using a Baldwin-Emery testing machine. The three surface textures were; (1) the as-received polished condition, (2) ground with 400 grit boron carbide abrasive and (3) ground with 80 grit silicon carbide abrasive. The padding material was annealed 1020 steel. The crosshead speed of the testing machine was 0.004 in/min. The sphere diameters were determined

by taking the average of ten measurements with a micrometer. The values for the loaded diameters were obtained by measuring the diameter of the indentation in the steel pads. The traveling stage microscope on a Tukon microhardness tester was used for these measurements. Magnification was 100 X.

Tensile strength values were calculated using the equation

$$\sigma = \frac{KP}{D^2} \qquad 5\text{-}7$$

where; P = measured load at failure

D = sphere diameter

K was taken from Figure B-2

Poisson's ratio of the glass spheres was found to be 0.2 by the resonant sphere technique.

The procedure used to measure diametrical compression strengths of boron suboxide and boron carbide was the same as that used for the glass spheres except that hardened 1020 and 4340 steel were used as pad materials. The 4340 steel was the hardest pad material used. It was used only for the boron carbide and high density boron suboxide specimens.

6. Results and Discussion

6-1 Elastic Properties of Polycrystalline Boron Suboxide

The effect of porosity on the room temperature elastic moduli of polycrystalline B_6O was investigated in the range of 0 to 16% porosity. Table 6-1 lists the calculated moduli and porosity data for 24 specimens of near stoichiometric B_6O. The data are segregated, however, into oxygen-rich (i.e., B_2O_3 second phase) and boron-rich groups. The concentration of second phase was always less than one volume percent as determined by chemical and/or metallographic and X-ray diffraction analyses. The elastic moduli of both groups exhibited the same dependence on porosity as can be seen in Figure 6-1.

The semi-log plots of Young's modulus and shear modulus indicate which of the empirical relations, discussed in Section 2-1, would best fit these data. The linear dependence of elastic modulus on porosity expressed by Equation (2- 8) produces a curve with an increasingly negative slope when ln M is plotted against porosity. The data plotted in Figure 6-1 indicate a decreasingly negative slope. An attempt to fit the exponential Equation (2- 7) would compromise the curvature of the data and predict a lower than observed zero porosity value. Hasselman's equation (2- 9) predicts the observed curvature. A least squares analysis of the data fit to Hasselman's equation

Table 6-1 Summary of the Elastic Moduli-Porosity Data for Near Stoichiometric B_6O

Vol. fraction porosity	Young's Mod (E) $\times 10^6$ psi	Shear Mod (G) $\times 10^6$ psi	Bulk Mod (K) $\times 10^6$ psi	Poisson's Ratio (ν)	Phases Present
0.081	46.7	20.2	22.9	0.156	
0.041	55.4	24.0	26.6	0.154	
0.031	56.4	24.4	27.4	0.156	
0.029	57.2	24.8	27.4	0.153	
0.028	58.0	25.2	27.7	0.153	
0.028	59.9	26.0	28.9	0.154	
0.028	57.7	25.0	28.0	0.156	
0.028	57.2	24.7	29.6	0.157	B_6O +
0.023	59.8	25.8	29.0	0.157	<1% B_2O_3
0.020	59.5	25.7	29.0	0.157	
0.018	61.5	26.6	29.8	0.156	
0.018	61.8	26.7	30.1	0.157	
0.017	61.1	26.4	30.2	0.155	
0.015	63.4	27.5	30.4	0.154	
0.013	62.0	26.8	30.1	0.156	
0.003	67.8	29.5	32.4	0.153	
0.001	68.8	29.9	32.8	0.153	
0.165	37.7	16.3	18.1	0.153	
0.134	37.8	16.4	18.0	0.153	
0.108	43.5	18.8	21.3	0.157	B_6O +
0.064	49.5	21.3	24.1	0.157	<1% Boron
0.007	65.9	28.5	31.9	0.156	
0.004	68.6	29.8	32.5	0.153	
0.000	69.1	29.9	33.3	0.154	

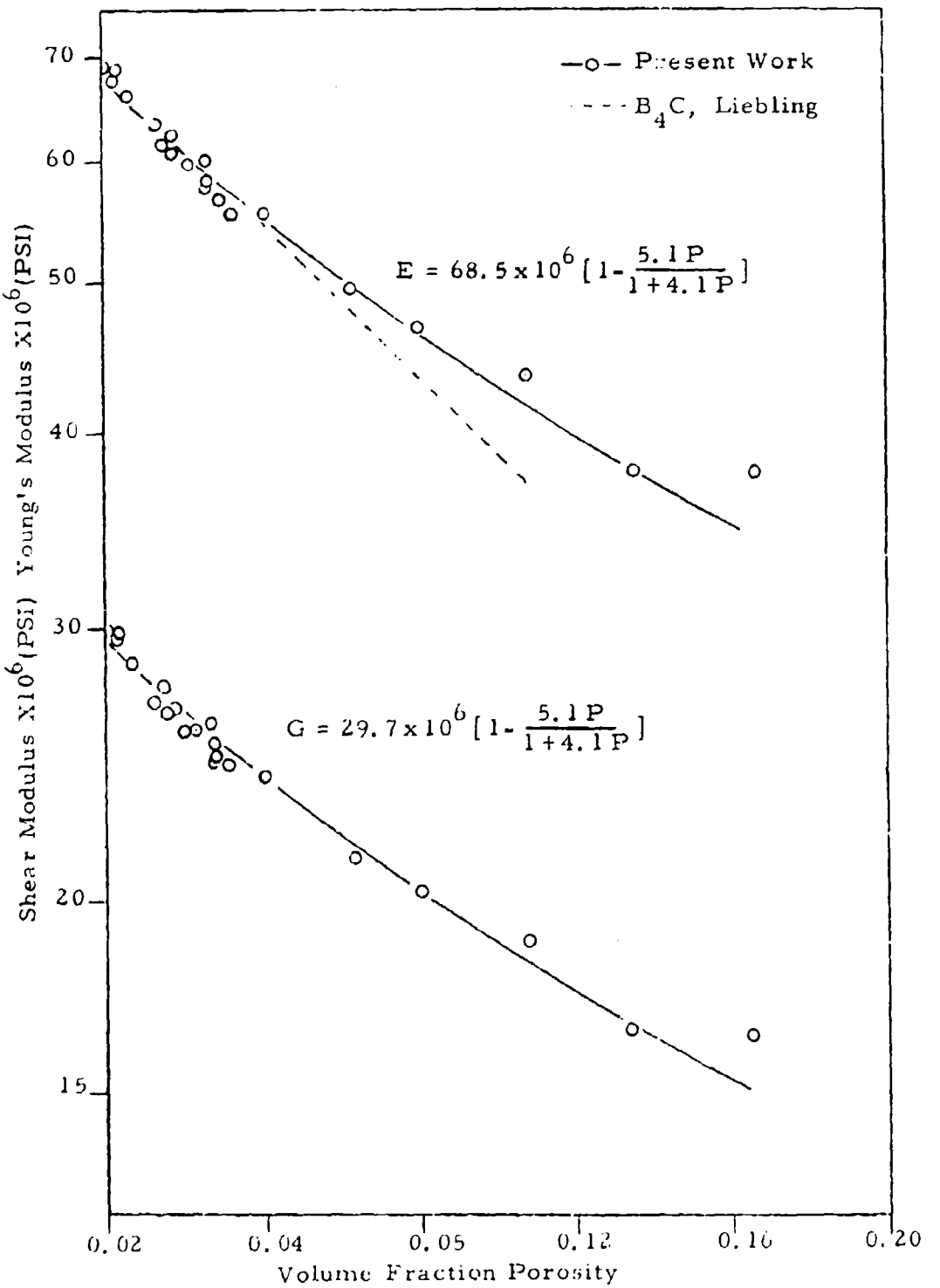

Figure 6-1. Young's and Shear Moduli versus Porosity for B_6O

gives $E_o = 68.5 \pm 0.5 + 10^6$ psi and $A = 5.1 \pm 0.1$.

Since Poisson's ratio was found to remain constant (within estimated experimental error) over the porosity range studied, the dependence of the shear modulus on porosity must be identical to that found for Young's modulus. Young's and shear moduli are related by the equation:

$$E = 2G(1+\nu) \qquad 6\text{-}1$$

If ν decreases with increasing porosity the effect of porosity on E will be greater than on G and vice versa.

The average value of Poisson's ratio was 0.155, and Hasselman's equation with A = 5.1 gives a zero porosity value of 29.7×10^6 psi for the shear modulus.

Since no other data for B_6O were found in the literature, a comparison was made with data for B_4C. This was reasonable since both materials are high boron compounds with nearly the same theoretical density ($\rho_o(B_6O) = 2.60$, $\rho_o(B_4C) = 2.52$ gm/cm^3) and probably the same crystal structure. Liebling[11] investigated the effect of porosity on Young's modulus of B_4C from 0 to 8% porosity. He measured Young's modulus for 29 hot pressed specimens by the resonant bar technique. The specimens were reported to have a uniform pore distribution and an average grain size of 7.4 μm. Liebling fitted his data to the linear relation (Equation (2-8)) and the exponential relation (Equation (2-7)) as well as a quadratic form. All three

relations were reported to fit the data equally well. The zero porosity values obtained from the three curve fits were averaged to give a value of 68.15×10^6 psi. Liebling's exponential curve is shown in Figure 6-1, and shows excellent agreement with the B_6O data between 0 and 6% porosity.

6-2 Verification of Tensile Fracture in Diametrically Compressed Brittle Spheres

Although the high speed moving film technique provided no information concerning the location of fracture initiation in the glass spheres, it did illustrate the explosive nature of a diametrically compressed sphere. Figure 6-2 shows two consecutive frames taken at 16,000 frames/sec. The first frame was taken sometime before fracture. Each frame had an exposure time of $\approx 6\,\mu$sec and $60\,\mu$sec was the time between frames. In less than $60\,\mu$sec the sphere was essentially pulverized. The finer powder (as fine as -325 mesh) remained in a small pile while the larger fragments (usually from the surface of the sphere) were found as far as 30 ft from the test position when the experiment was not shielded. Four attempts at 32,000 frames per second showed the same results.

The method of taking single photographs in a darkened room gave much more informative pictures. Figure 6-3 shows four glass spheres being diametrically compressed under a distributed load. The

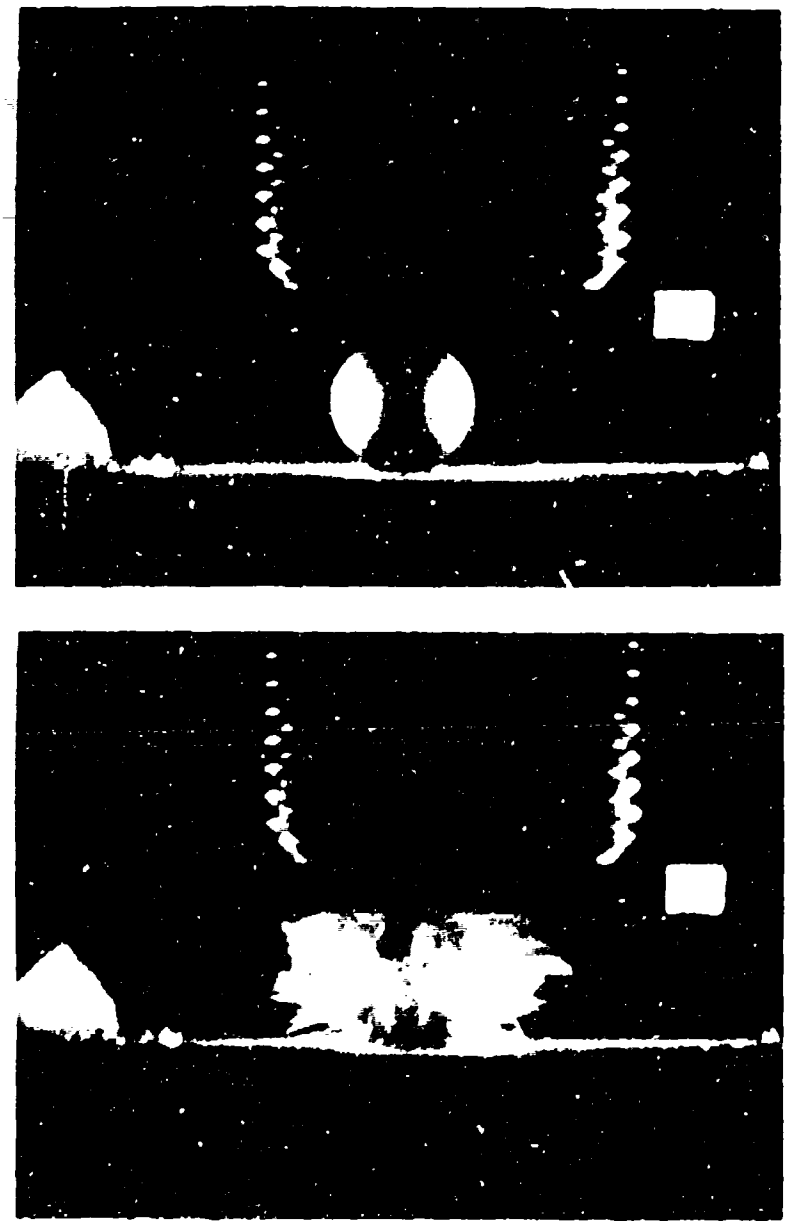

Figure 6-2. High speed movies of a diametrically compressed glass sphere. Two consecutive frames taken at 16,000 frames per second.

Figure 6-3a

Figure 6-3b

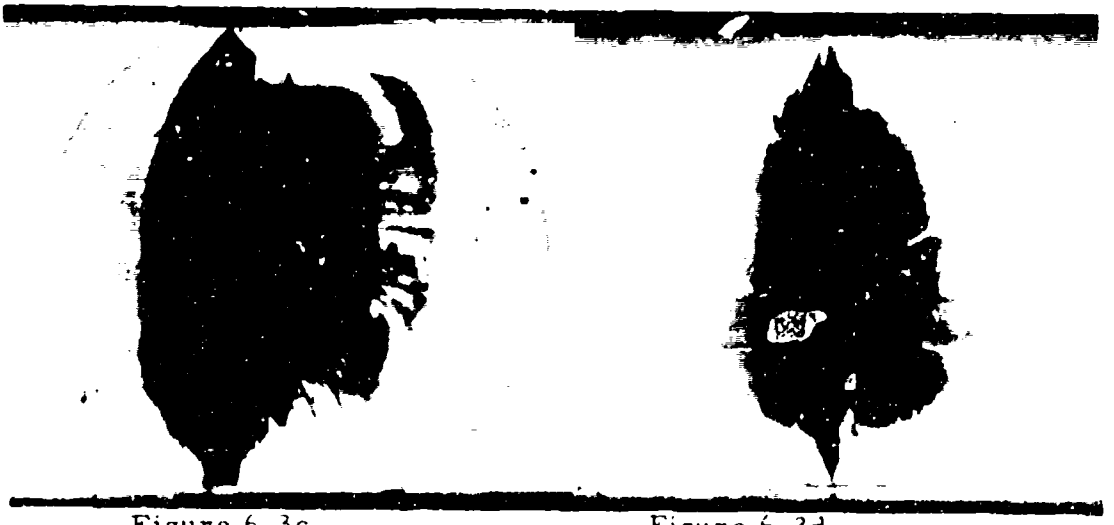

Figure 6-3c

Figure 6-3d

Fifure 6-3. Photographs of diametrically compressed glass spheres. Figures 6-3b, c, and d were taken approximately 3 μsec after fracture initiation.

photograph in Figure 6-3a was taken before fracture by externally interrupting the laser beam. The dark spots on the sphere were air bubbles in the glycerol. Figures 6-3b, c and d are photographs taken by loading the spheres to failure. It is logical to assume the darkened areas were caused by reflection and scattering of light due to interfaces created in the sphere. The darkened areas, therefore, indicate the general location of fracture initiation, i.e., along the loaded diameter near the center of the sphere. This was also the region of maximum tensile stress.

The streak of light which is most prominent in Figure 6-3b was observed upon fracture of all the borosilicate glass spheres. This emission of light during a tensile failure in borosilicate glass was also observed by Outwater [38], who described this phenomenon as triboluminescence. Outwater found triboluminescence to occur when a tensile failure initiated beneath the surface in compressively loaded necked specimens. The fragments of specimens fractured under these conditions were described by Outwater as a "coherent, white mass of glass." The interior of diametrically compressed glass spheres, tested in air, was also reduced to a fine, white powder.

Although the photographs shown in Figure 6-3 and the similarities found with Outwater's work certainly indicate the location for fracture initiation, the measurement of tensile strength on glass spheres with different surface conditions demonstrated that fracture was not

initiated on the surface. The results of these strength tests are shown in Table 6-2.

The average values of tensile strength for the polished and 400 grit surfaces showed good agreement at 7.41 and 7.50 ksi, respectively. The slightly higher average value of strength, 7.80 ksi, found for the 80 grit surface indicates the independence of this test method on surface conditions; thus fracture was not initiated at a surface.

The 5% deviation in measured strength values is not unreasonable for materials such as glass. The average value for all 16 specimens was 7.57 ksi and all the data were within a total range of 12% of the average. This relatively small deviation was probably due to increased frictional forces at the contact area caused by the extremely rough sphere surface. A tendency to direct the loading toward the center of the sphere, rather than the assumed uniaxial compression, occurs when friction at the contact area is high.

The use of a metal pad to distribute the load always tends to distort the assumed stress distribution slightly; however, high frictional forces and loaded diameter to sphere diameter ratios greater than 0.36 probably introduce significant errors. Although no successful attempt was made to determine the magnitude of these errors, the effect is to predict tensile strengths which are too high. One way to deal with this problem might be to grind two parallel and equal areas on the sphere and use harder metal pads, but this may create stress concentrations due to misalignment.

Table 6-2 Summary of Tensile Strength Data on Diametrically Compressed Glass Spheres with Different Surface Textures

Sphere Dia. (in.)	Load (P) (lb.)	Loaded Dia. / Sphere Dia.	K	Strength (σ) (ksi)	Ave. Strength ($\bar{\sigma}$) (ksi)
		Polished Surface			
0.375	1790	0.273	0.60	7.67	
0.375	1750	0.266	0.61	7.57	
0.375	1670	0.263	0.62	7.35	7.41
0.375	1650	0.264	0.62	7.20	
0.375	1670	0.266	0.61	7.23	
0.375	1760	0.274	0.60	7.49	
		400 Grit Surface			
0.375	1770	0.280	0.59	7.[illegible]	
0.373	1780	0.275	0.60	[illegible]	7.50
0.374	1700	0.272	0.60	[illegible]	
0.375	1770	0.276	0.60	7.55	
		80 Grit Surface			
0.375	1700	0.263	0.62	7.50	
0.375	1870	0.275	0.60	7.98	
0.375	1760	0.275	0.60	7.51	7.80
0.374	1730	0.259	0.62	7.73	
0.375	1960	0.288	0.58	8.08	
0.375	1900	0.281	0.59	7.97	

6-3 Tensile Strength of Boron Suboxide by Diametrical Compression of Spheres

Tensile strength measurements were also made on the boron suboxide spheres after the elastic properties evaluation. Since the spheres were of varying porosities, an evaluation of the effect of porosity on the tensile strength was obtained. Table 6-3 shows the results of the strength measurements. Two spheres of boron carbide were also tested and the results shown in Table 6-3.

As discussed in the previous section, the effect of increasing the loaded diameter to sphere diameter ratio would be to distort the assumed stress distribution and to obtain higher than expected strength values. Although the maximum acceptable value of 0.36 for this ratio was somewhat arbitrarily chosen, it was observed that ratios of 0.4 to 0.5 gave strength values as high as 55 ksi for low porosity ($P < 0.04$) boron suboxide specimens. This presented somewhat of an experimental problem in that some estimate of the strength had to be made in order to choose the proper pad material. A number of spheres were essentially wasted in order to arrive at the conclusion that hardened 4340 steel (Rockwell C hardness = 57) should be used for higher strength specimens and hardened 1020 steel (Rockwell C hardness = 30) should be used for the lower strength specimens. In a few cases, however, when the strengths of the specimens were overestimated, loaded diameter to sphere diameter ratios less than 0.18 and very

Table 6-3 Summary of Tensile Strength Data on Diametrically Compressed B_6O and B_4C Spheres

Sphere Dia (in.)	Load (P) (lb)	$\frac{\text{Loaded Dia}}{\text{Sphere Dia}}$	K	Strength (σ) (ksi)	Porosity
		Boron Suboxide			
0.397	11,000	0.313	0.605	42.2	0.0
0.314	5,080	0.245	0.79	35.6	0.0
0.159	1,650	0.324	0.59	38.4	0.021
0.240	3,670	0.359	0.56	36.7	0.028
0.293	5,930	0.325	0.59	40.7	0.028
0.260	4,140	0.304	0.62	38.0	0.019
0.332	5,420	0.282	0.65	32.0	0.064
0.305	3,300	0.313	0.605	21.5	0.135
0.352	3,820	0.305	0.620	19.1	0.164
		Boron Carbide			
0.267	5,610	0.357	0.56	43.3	0.004
0.257	5,690	0.316	0.60	51.7	0.004

low calculated strengths were obtained. These low values were always associated with a surface related failure, i.e., fragments appeared to spall off the surface just outside the area of contact. The explosive type of failure, described earlier for glass spheres, was always observed for loaded diameter to sphere diameter ratios greater than 0.18. The above discussion indicates that, for specimens with Poisson's ratio ≈ 0.15, the range of loaded diameter to sphere diameter ratio should be restricted to 0.18 to 0.36. A few cursory tests of alumina spheres, not reported here, indicated this range may be extended to as low as 0.14 for Poisson's ratio of 0.24.

The data from Table 6-3 are plotted in Figure 6-4 along with some preliminary flexural strength data on boron suboxide. The flexural data[39] was obtained by four point bend tests on specimens 0.1 x 0.2 x 0.15 inches cut from hot pressed billets. The source of material for the flexural specimens was identical to that for the spheres. The curves for each set of data were best fit by inspection.

Although the strength values measured by the compression of spheres were 25 to 30% lower than the flexural data, the predicted dependences of strength on porosity were in reasonable agreement. The equations for the two curves are also shown in Figure 6-4. The average strength of two spheres of boron carbide was found to be approximately 10% higher than the zero porosity value of boron suboxide spheres.

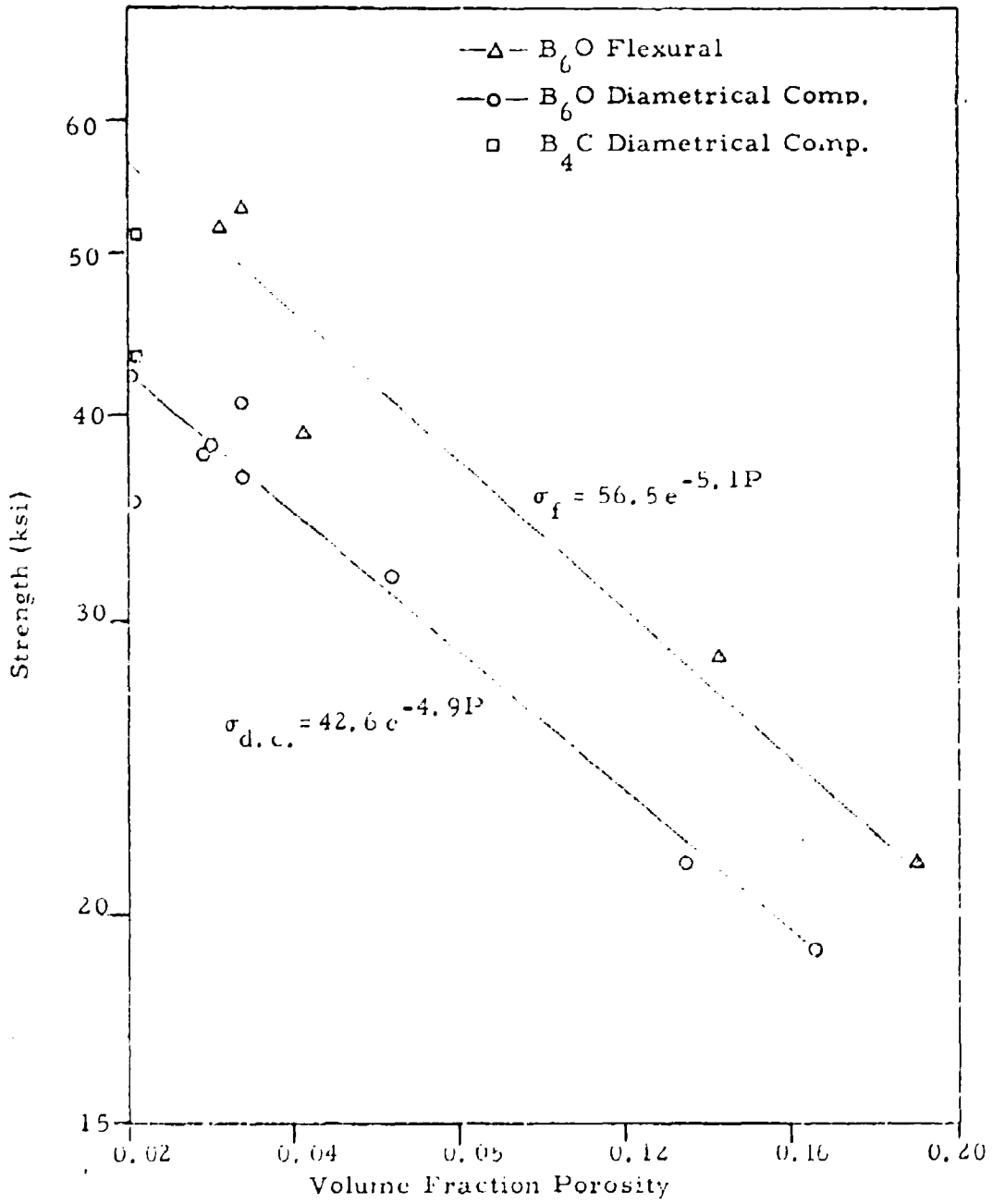

Figure 6-4. Diametrical Compression Strength of B_6O and B_4C versus Porosity and Flexural Strength of B_6O versus Porosity

The relatively low degree of scatter encountered for diametrical compression data was somewhat surprising since each data point represents only one test specimen. Each data point on the flexural curve represents between 3 to 10 tests. The consistency observed for the diametrical compression data may, of course, be fortuitous in light of the small number of tests reported. It should be pointed out that the relatively small specimen sizes tested provide an even smaller volume of material near the region of maximum tensile stress. Based on the Weibull probability theory, consistent results would be expected. It should also be emphasized that a number of specimens were rejected on the basis of unacceptable loaded diameter to sphere diameter ratios.

Surface cracks due to machining damage are normally considered to be the controlling parameters for flexural strength measurements. With this in mind, it might be expected that strength values for the diametrically compressed spheres (where fracture is initiated below the surface) should be higher than flexural values. The observed relationship between these values can, however, be explained. Flexural tests produce uniaxial stress states; whereas, the diametrical compression of a sphere produces a triaxial stress state. It is well known that theoretical mechanics predicts a lower failure stress for the triaxial stress state than for the uniaxial stress state.

7. Summary

The effect of porosity on the dynamic elastic moduli of polycrystalline boron suboxide (B_6O) has been determined at room temperature. The dependence of Young's and shear moduli on porosity were found to follow Hasselman's semi-empirical relation with $E_o = 68.5 \times 10^6$ psi and $A = 5.1$. Based on the elasticity data obtained in this study and the known values of theoretical density and microhardness, boron suboxide should be nearly equivalent to boron carbide as a ceramic armor material. Ballistic testing, however, is needed to substantiate this.

The diametrical compression of a sphere, under the proper conditions, has been shown to provide a new tensile strength test for brittle materials in which fracture is initiated beneath the specimen surface. High speed photographic studies on glass spheres demonstrated that fracture initiates near the center of the sphere which is the location of maximum tensile stress. Strength values obtained by this method were shown to be independent of surface finish, and to be lower than flexural strength values.

This test method may be used to more closely approximate unusual stress conditions such as those encountered during ballistic impact. It may be useful for obtaining mechanical properties data when only small specimen sizes are available, particularly when used in conjunction with the resonant sphere technique for elastic properties. This method also has the capability of measuring, comparatively at

least, intrinsic properties of a material rather than surface effects of machining.

Further research should be directed toward determining the limits of load distribution and the effect of Poisson's Ratio on those limits. Also it may be possible to evaluate the triaxial stress state such that the equivalent uniaxial stress for failure may be predicted.

8. Conclusions

1. The dependence of Young's Modulus on porosity for the porosity range 0 to 16% was found to follow the relation

$$E = 68.5 \times 10^6 \text{ psi } [1 - \frac{5.1P}{1+4.1P}]$$

2. Photographs of a diametrically compressed glass sphere taken $\approx 3\mu$ sec after fracture initiation showed that fracture initiation occurred near the center of the sphere which is the region of maximum predicted tensile stress.

3. Tensile strength measurements on diametrically compressed glass spheres were found to be independent of surface finish.

4. Tensile strength values obtained by diametrically compressing boron suboxide spheres were found to be 25 to 30% lower than four point bend strengths on the same material.

5. The range of acceptable load distribution, i.e., loaded diameter to sphere diameter ratio was found to be 0.2 to 0.36 for boron suboxide spheres.

Bibliography

1. Mackenzie, J.K., The Elastic Constants of a Solid Containing Spherical Holes, Proc. Phys. Soc. (London) Series B, 62, 2-11 (1950).

2. Coble, R.L. and Kingery, W.D., Effect of Porosity on Physical Properties of Sintered Alumina, J. Am. Ceram. Soc., 39, 377-385 (1956).

3. Paul, B., Prediction of Elastic Constants of Multiphase Materials, Trans. AIME, 218, 36-41 (1960).

4. Hashin, Z., The Elastic Moduli of Heterogeneous Materials, J. Appl. Mech., March, 143-150 (1962).

5. Buch, A. and Goldschmidt, S., Influence of Porosity on Elastic Moduli of Sintered Materials, Mat. Sci. and Eng., 5, 111-118 (1969/70).

6. Wachtman, J.B., Tefft, W.E., Lam, D.G., and Stinchfield, R.P., Elastic Constants of Synthetic Single Crystal Corundum at Room Temperature, J. Res. Natl. Bur. Std., A, 64, 213 (1960).

7. Soga, N. and Anderson, O.L., High-Temperature Elastic Properties of Polycrystalline MgO and Al_2O_3, J. Am. Ceram. Soc., 49 [7] 355-59 (1966).

8. Rankin, D.T., Stiglich, J.J., Petrak, D.R., and Ruh, R., Hot-Pressing and Mechanical Properties of Al_2O_3 with an Mo-Dispersed Phase, ibid, 54 [6] 276-81 (1971).

9. Spriggs, R.M., Expression for the Effect of Porosity on Elastic Modulus of Polycrystalline Refractory Materials, Particularly Aluminum Oxide, ibid, 44 [12] 628-29 (1961).

10. Powell, B.R., Orville, H., and Manning, W.R., Elastic Properties of Polycrystalline Ytterbium Oxide, ibid, 54 [10] 488-90 (1971).

11. Liebling, R.S., Effect of Low Porosity on the Elastic Properties of Boron Carbide, Mat. Res. Bull., Vol. 2, 1035-40 (1967).

12. Petrak, D. R. and Rankin, D. T., Effect of Porosity on the Elastic Moduli of $CoAl_2O_4$ and CoO-MgO Solid Solutions, To be presented at the 74th Annual Meeting of the American Ceramic Society, May 1972.

13. Hasselman, D. P. H., Porosity Dependence of the Elastic Moduli of Polycrystalline Refractory Materials, J. Am. Ceram. Soc., 45 [9] 452-53 (1962).

14. Weintraub, E., Trans. Am. Electrochem. Soc., 16, 165-184, (1909).

15. Kahlenberg, H. K., ibid, 47, 23-62 (1926).

16. Holcombe, C. E. and Horne, O. J., Preparation of Boron Suboxide, B_7O, J. Am. Ceram. Soc., 55 [2] 160 (1972).

17. Pasternak, R. A., Acta Cryst., 12, 612-13 (1959).

18. LaPlaca, S. and Post, B., Planseeber Pulvermet, Bd 9, 109-12 (1961).

19. Post, B., Refractory Binary Borides, in Roy M. Adams, Ed., Boron, Metalloboron Compounds, Interscience Publishers, New York, 1964, pp 301-71.

20. Rizzo, H. F., J. Electrochem. Soc., 109, 1079-82 (1962).

21. Silver, H. A. and Bray, P. J., J. Chem. Phys., 11, 247 (1959).

22. Hoard, J. L. and Hughes, R. E., Elementary Boron and Compounds of High Boron Content: Structure, Properties and Polymorphism, in E. L. Muetterties, The Chemistry of Boron and Its Compounds, John Wiley and Sons, Inc., New York, 1967, pp 25-154.

23. Matkovich, V. I., J. Am. Chem. Soc., 83, 1804-1806 (1961).

24. Glaser, F. W., Moskowitz, and Post, B., J. Appl. Phys., 24, 731 (1953).

25. Longuet-Higgins, H. C. and Roberts, M. deV., Proc. Roy. Soc. (London) 230A, 110-19 (1955).

26. Private Communication, R. Novak, RCA Laboratories, Princeton, N. J.

27. Private Communication, P. W. R. Corfield, Chemistry Dept., Ohio State University, Columbus, Ohio.

28. Domagala, R. F. and Ruh, Robert, ASM Trans Quart., 62, 915-925 (1969).

29. Baun, W. L. and Solomon, J. S., Boron Bonding Studies Using the Electron Probe. Presented at the Twenty-Second Pittsburgh Conference on Analytical Chemistry and Applied Spectroscopy, Cleveland, Ohio, Feb. 28-March 5, 1971.

30. Private Communication, C. M. Phillipi, Analytical Branch, Air Force Materials Laboratory, Wright-Patterson Air Force Base, Ohio.

31. Carbonara, R. S. and Alexander, C., Letter Report on Contract F33615-71-C-1070, Preliminary Experiments on the High Temperature Behavior of Boron Suboxide, Sept. 3, 1971, Battelle Columbus Laboratory, Columbus, Ohio.

32. Inghram, M. G., Porter, R. F., and Chupka, J., J. Chem. Phys., 25, 498-501 (1956).

33. Petrak, D. R., Ruh, R., and Goosey, E., Presented at the National Bureau of Standards 5th Materials Symposium - Solid State Chemistry (October 1971). Proceedings to be published by National Bureau of Standards.

34. Private Communication, W. B. Shook, Department of Ceramic Engineering, Ohio State University.

35. Hiramatsu, Y. and Oka, Y., Determination of the Tensile Strength of Rock by a Compression Test of an Irregular Test Piece, Int. J. Rock Mech. Min. Sci., Vol. 3, 89-99 (1966).

36. Fraser, D. B. and LeCraw, R. C., Novel Method of Measuring Elastic and Anelastic Properties of Solids, Rev. Sci. Inst., 35, 1113 (1964).

37. Schreiber, E., Anderson, O. L., and Soga, N., Elastic Constants and Their Measurement, Final Report AFML-TR-65-202.

38. Outwater, J.O. and Gerry, D.J., The Effects of High Uniaxial Compressive Stress on Glass, Research Memorandum for Contract NONR-3219(01)(x) Aug 10, 1966. AD 640 847.

39. Private Communication, R. Ruh, D. Petrak and G. Atkins, Air Force Materials Laboratory, Wright-Patterson AFB, Ohio.

40. Love, A.E.H., A Treatise on the Mathematical Theory of Elasticity, Dover Publications, New York (1944).

41. Sato, Y. and Usami, T., Torsional Oscillation of a Homogeneous Elastic Spheroid, Bull. Seismol, Soc. Am., 52, 469-84 (1962).

42. Ceramic-Armor Technology, DCIC Report 69-1, Part I, May, 1969.

43. Frocht, M.M., Photoelasticity, John Wiley and Sons, Inc., 1941.

44. Timoshenko, S. and Goodier, J.N., Theory of Elasticity, McGraw-Hill Book Company, 1951.

APPENDIX A

Resonant Sphere Technique for Elastic Properties

This method of determining the elastic constants of small specimens was first presented by Fraser and LeCraw [36] then further evaluated by Schreiber, Anderson and Soga. [37] The following is a summary of the theory and equipment for this method as presented by Schreiber et al.

A-1 Free Oscillations of an Isotropic Sphere

The equations of motion for the free oscillations of an isotropic elastic sphere have been evaluated by many authors. Love [40] has presented a detailed derivation which is far more than need be included here. Schreiber et al. have summarized the derivation sufficiently to understand the experimental procedure and to perform the necessary calculations.

The equations for small oscillations of an isotropic elastic body are given by

$$\rho\left(\frac{\partial^2 u}{\partial t^2}, \frac{\partial^2 v}{\partial t^2}, \frac{\partial^2 w}{\partial t^2}\right) = (\lambda + G)\left(\frac{\partial \Delta}{\partial x}, \frac{\partial \Delta}{\partial y}, -\frac{\partial \Delta}{\partial z}\right) + \mu \nabla^2 (u, v, w) \qquad \text{A-1}$$

where u, v, and w are x, y, and z components of the displacement U, G and λ are the shear moduli and Lamé's constant and

$$\Delta = \frac{\partial u}{\partial x} + \frac{\partial v}{\partial y} + \frac{\partial w}{\partial z} \qquad \text{A-2}$$

For an elastic body U may be expressed by

$$U = A e^{2\pi i w t} \qquad \text{A-3}$$

Equation A-1 can then be rewritten as

$$(\nabla^2 + h^2)\nabla = 0 \qquad \text{A-4}$$

where $h = (2\pi w)^2 / \frac{\lambda + 2G}{\rho}$ A-5

For a body of spherical symmetry, Equation A-5 can be separated into two functions; one dependent on the radius, the other on the angular coordinates. The angular function can be expressed as a sum of surface spherical harmonics by $R_\ell(\gamma) P_\ell^m (\sin \Theta) e^{i m \phi}$, where P_ℓ^m is the associated Legendre function, the integers ℓ and m denote the order of the spherical harmonic with respect to the angular coordinates ϑ and φ. Another integer associated with the radial function is also required. This integer, usually signified by n, determines the number of nodal surfaces for a given vibrational mode. The notation used previously and adopted here is nS_ℓ^m for spheroidal modes and nT_ℓ^m for torsional modes. Since for this application only the lower nS_ℓ^0 and nT_i^0 modes are normally considered, the m is deleted and assumed zero.

Torsional vibrations are pure shear modes, i.e., no radial displacements occur. The displacement at any point is directed at right angles to the radius of the sphere. The characteristic equation for the ℓth harmonic of the torsional oscillations is

$$(\ell - 1)\psi_{\ell}\ (ka) + ka\psi'_{\ell}\ (ka) = 0 \qquad \text{A-6}$$

where a is the radius, ka is 2π x frequency x shear velocity, and $\psi_{\ell}\ (\chi)$ is a function expressible in terms of a Bessel's function by the formula

$$\psi_{\ell}\ (\chi) = (-1)^{\ell} \sqrt{\frac{2}{\pi}}\ \chi^{-(\ell + \frac{1}{2})} J_{\ell + \frac{1}{2}}(\chi) \qquad \text{A-7}$$

Equation (A-6) now becomes

$$(\ell - 1)\ J_{\ell + \frac{1}{2}}(ka) - ka\ J_{\ell + \frac{3}{2}}(ka) = 0 \qquad \text{A-8}$$

Some of the numerical solutions to this equation were obtained by Sato and Usami[41] for ka, and they are listed in Table A-1. Figure A-1 shows a schematic representation of a few torsional modes.

The spheroidal oscillations involve both transverse and radial components of the shear velocity, v_s, and longitudinal velocity, v_p. By using a quantity $ha = 2\pi w v_p$ the characteristic equation to be solved is of the form

$$\frac{2h}{k}\left[\frac{1}{ka} + \frac{(n-1)(n+2)}{(ka)^2}\ \frac{J_{n-3/2}(ka)}{J_{n+3/2}(ka)} - \frac{n+1}{ka}\right] J_{n+3/2}(ha)$$

$$+\left[-\frac{1}{2} + \frac{(n-1)(2n+1)}{(ka)^2} + \frac{1}{ka}\left(1 - \frac{2n(n-1)(n+2)}{(ka)^2}\right)\ \frac{J_{n+3/2}(ka)}{J_{n+1/2}(ka)}\right] J_{n+\frac{1}{2}}(ha)$$

$$= 0 \qquad \text{A-9}$$

To solve this equation numerically the ratio h/k must be known. Since h/k is expressible in terms of Poisson's ratio, γ, ha can be calculated for any value of γ using equation (A-9), and

Table A-1 Nondimensional Frequency of Torsional Oscillation (ka); n^{T}_{ℓ} of a Homogeneous Sphere.

	n = 1				
ℓ = 1	-----	5.7635	9.0950	12.3229	15.5146
2	2.5011	7.1360	10.5146	13.7717	16.9831
3	3.8647	8.4449	11.8817	15.1754	18.4121
4	5.0946	9.7126	13.2109	16.5445	19.8094
5	6.2658	10.9506	14.4108	17.8858	21.1806
6	7.4036	12.1664	15.7876	19.2042	22.5298
7	8.5199	13.3646	17.0463	20.5034	23.8601
8	9.6210	14.5484	18.2871	21.7	
9	10.7109	15.7204	19.5152	23.0545	
10	11.7921	16.8821	20.7315	24.3104	

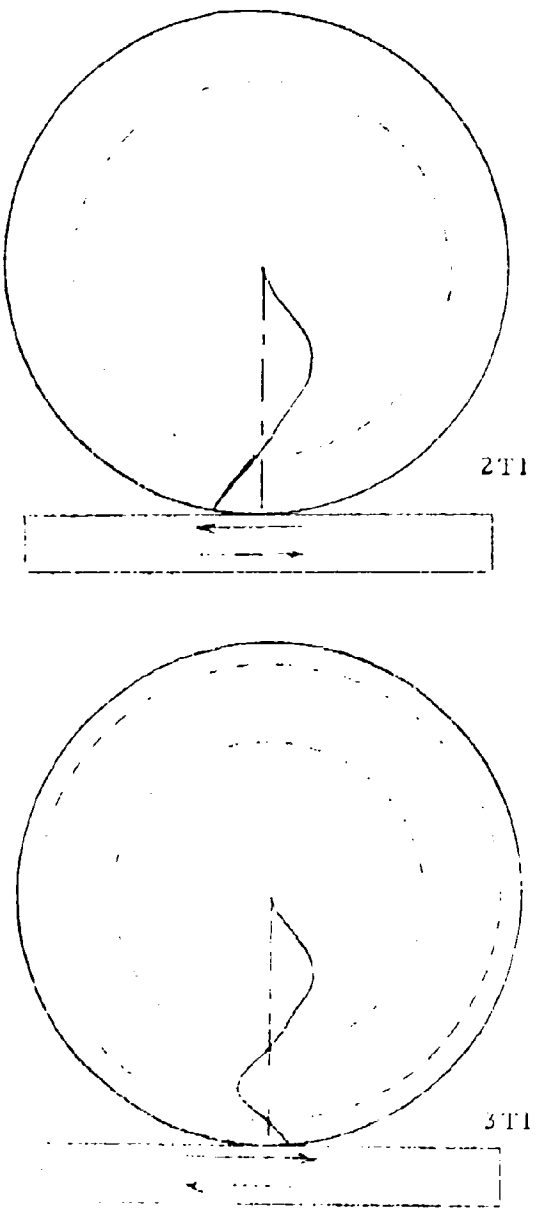

Figure A-1 Schematic Representation of Two Torsional Modes.

$$\frac{h^2}{k^2} = (1-2\nu)/2(1-\nu) \qquad \text{A-10}$$

Sato and Usami[41] have also calculated values of ha for a number of aSt modes at a few values of Poisson's ratio, and they are shown in Table A-2. Fraser and LeCraw, however, have performed more extensive computations and constructed the set of curves shown as Figure A-2.

The values of ha and ka can be thought of as nondimensional frequencies. The quantities π/ha and π/ka are the ratios of the period of oscillation to the time taken for a transverse or shear wave to traverse a distance equal to the diameter of the sphere. If the frequency (f) of a particular torsional mode is measured, the shear velocity of sound of the material can be calculated from the diameter of and

$$V_s = \pi f d/(ka) \qquad \text{A-11}$$

A-2 Equipment and Operation

The equipment used in this study had been previously built by E. Schreiber for the Air Force Materials Laboratory. A list of parts as given by Schreiber et al. is given in Table A-3 and a schematic wiring diagram is shown in Figure A-3.

Referring to Figure A-3, the signal from the frequency generator is first amplified and then sent on to an electronic switch which is constantly being triggered on and off by the gate from the

Table A-2 Nondimensional Frequency of Spheroidal Oscillation ($h a$), n^{S}_{ℓ}, of a Homogeneous Sphere.

	Poisson's Ratio				
Mode	0.10	0.17	0.25	0.33	0.40
1^{S}_{0}	3.3977	3.8071	4.4400	5.4322	7.0952
1^{S}_{2}	2.6152	2.6279	2.6399	2.6497	2.6569
1^{S}_{3}	3.8360	3.8771	3.9163	3.9489	3.9731
1^{S}_{4}	4.8747	4.9425	5.0093	5.0662	5.1090
1^{S}_{5}	5.8511	5.9416	6.0327	6.1118	6.1722
2^{S}_{1}	3.0737	3.2424	3.4245	3.5895	3.7168
2^{S}_{2}	4.4129	4.6263	4.8653	5.0878	5.2619
2^{S}_{3}	5.9597	6.1924	6.4544	6.6959	6.8811
3^{S}_{1}	5.8951	6.2383	6.7713	7.2306	7.3705

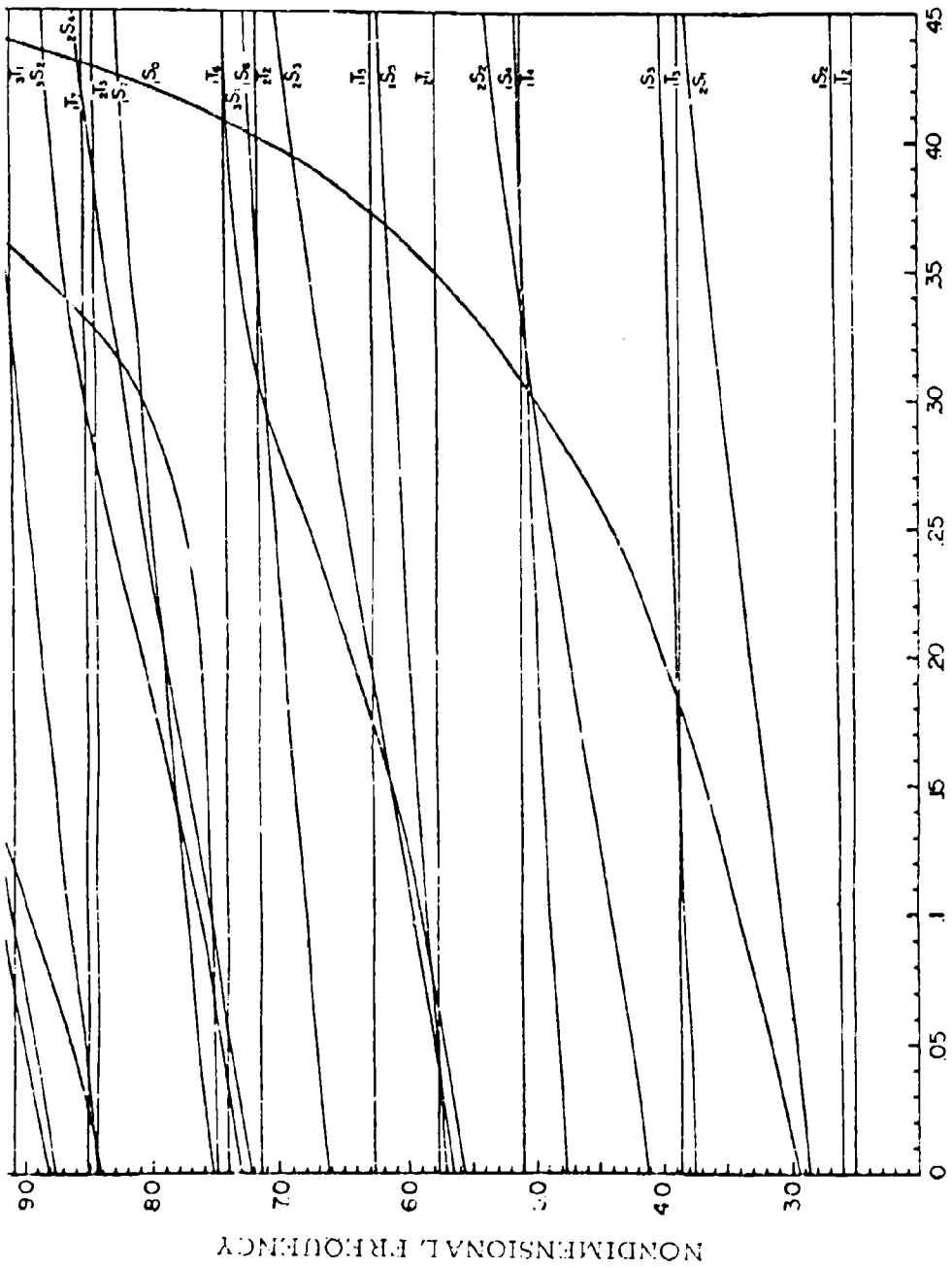

Figure A-2. Nondimensional frequency versus Poisson's Ratio

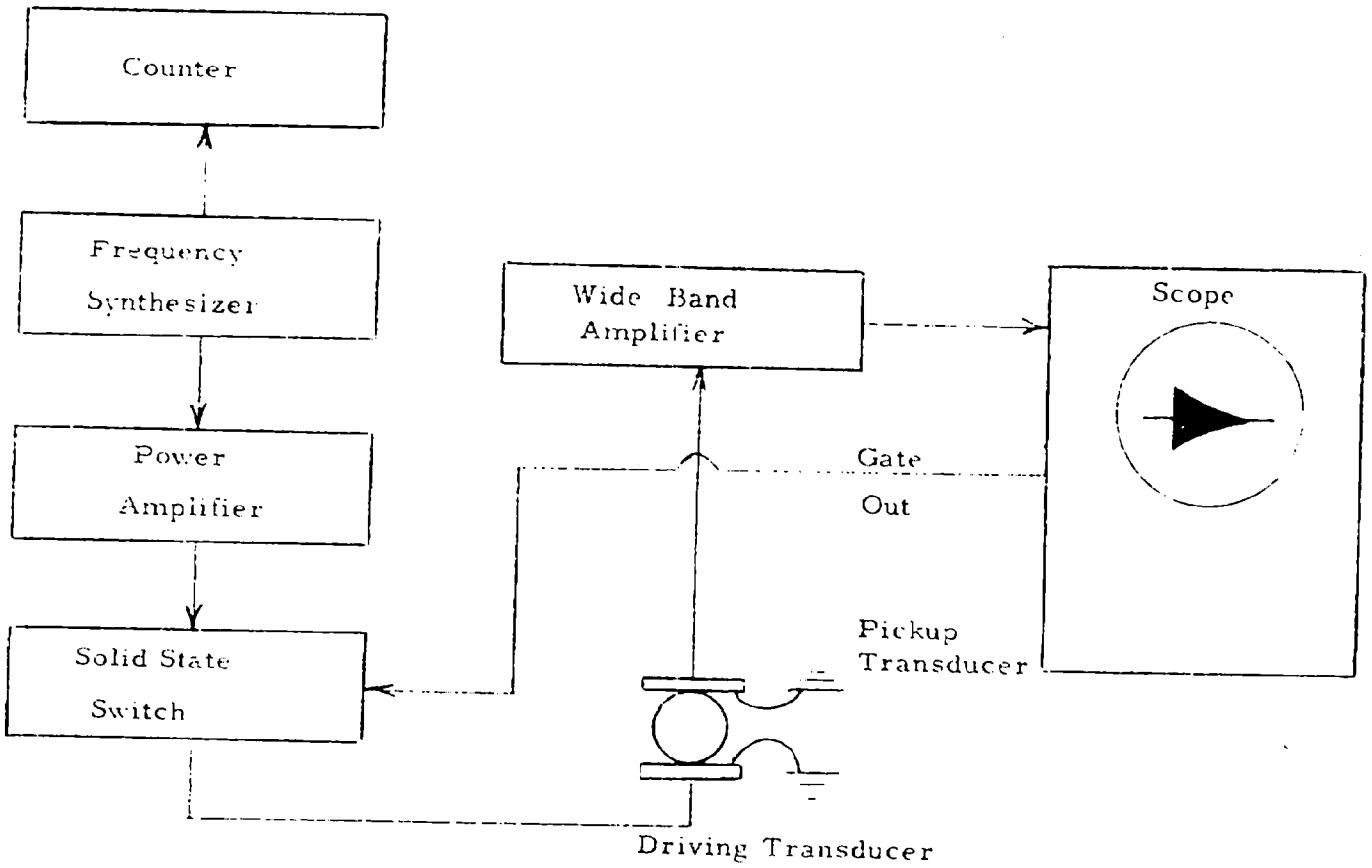

Figure A-3 Block Diagram of Electronic System for the Resonant Sphere Technique.

Table A-3 Description of Equipment Requirements

For the Resonant Sphere Technique

Component	Requirements	Presently Used Component
Frequency Counter	Should read out to Hz, from 0 to 5 MHz	Hewlett-Packard Model 5244L
Frequency Generator	Continuous and stable frequency control from 0.1 to 3 MHz and controllable output to 2 volts on a 50 ohm load.	Rhode and Schwartz XUA synthesizer
Solid State Switch	Single-pale double-throw with high isolation	Sander Associates Model DS-16
Amplifier	Wide band amplifier	Hewlett-Packard Model 462A
Oscilloscope	Dual time base dual channel	Tektronix type RM 35A
Transducers	Shear mode transducers with resonant frequencies between 1 to 3 MHz	Gulton Industries Glennite Piezoceramics Catalog No. P/N 3P1-HST-21

oscilloscope. When the switch is in the "ON" position the signal goes to the driving transducer which vibrates the sphere. When the switch is in the "OFF" position, no signal is sent to the driver. The signal from the pickup transducer is amplified and displayed on the oscilloscope. If the frequency with which the sphere was vibrated (with switch "ON") was a resonant frequency, a decay pattern will be displayed (when the switch is "OFF"). If the vibrating frequency was not a resonant frequency, no pattern is displayed. Figures A-4 and A-5 show the resonant and nonresonant conditions, respectively.

The detection of the resonant condition can be monitored by watching the oscilloscope or by using an X, Y recorder. In either case the precise reading of the resonant frequencies should determine using a frequency counter and careful manual adjustment.

Although it was not considered in this investigation, this equipment is capable of providing information about internal damping. A simple R C circuit with variable resistor provides a source of variable electronic Q. When the decay patterns are displayed simultaneously (o. a dual trace oscilloscope) an estimation of the internal friction of the sphere is possible. See Fraser and LeCraw [36] for further details.

Table A-4 is included in this Appendix to show the relationships between the elastic moduli of isotropic bodies. As can be seen from

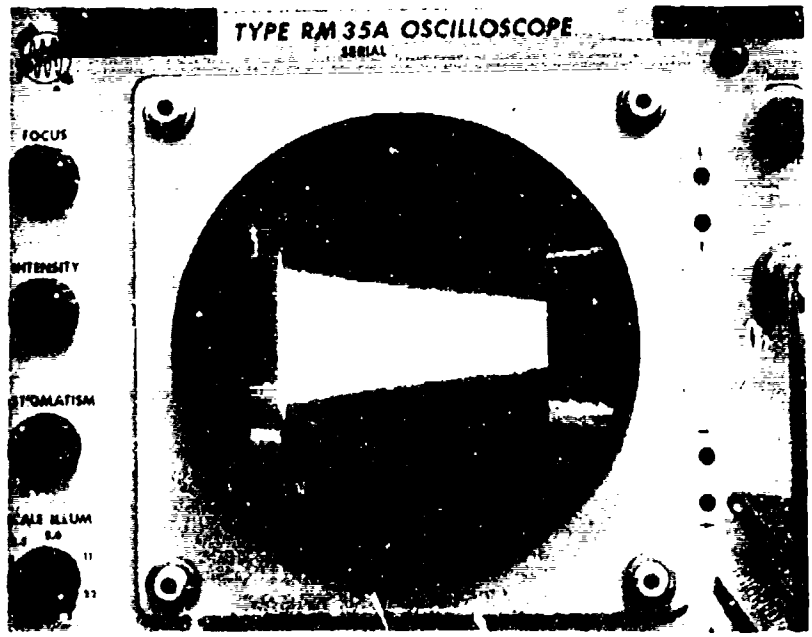

Figure A-4. Oscilloscope pattern showing resonant condition.

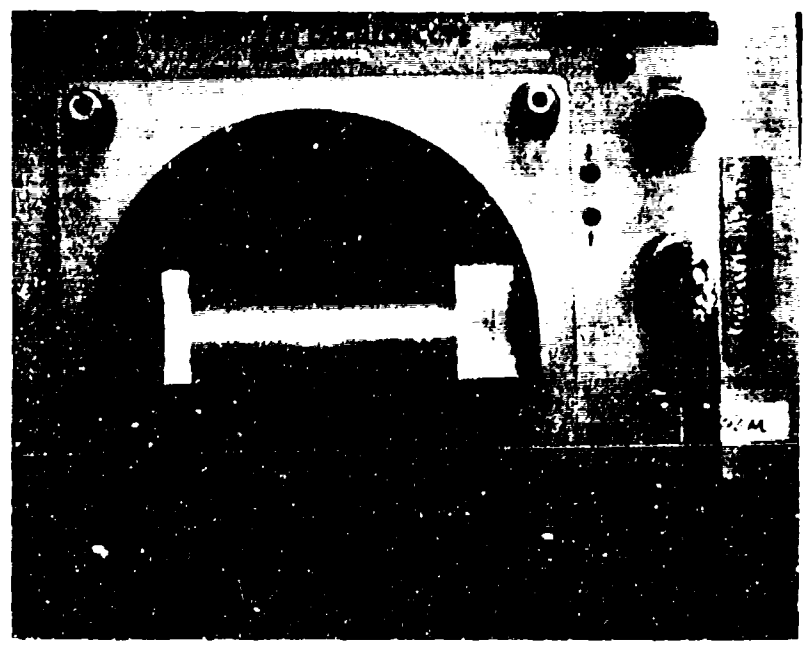

Figure A-5. Oscilloscope pattern showing nonresonant condition.

the table, when any two moduli are known the other four can be calculated.

Table A-4 The Relationships Between Elastic Constants of Isotropic Bodies*

Bulk (K)	Young's (E)	Lamé's Constant (λ)	Poisson's Ratio (ν)	Longitudinal (ℓ)	Shear (G)
$\lambda + 2G/3$	$G\,\frac{3\lambda+2G}{\lambda+G}$	....	$\frac{\lambda}{2(\lambda+G)}$	$\lambda+2G$	....
....	$9K\,\frac{K-\lambda}{3K-\lambda}$	....	$\frac{\lambda}{3K-\lambda}$	$3K-2\lambda$	$3(K-\lambda)/2$
....	$\frac{9KG}{3K+G}$	$K-2G/3$	$\frac{3K-2G}{2(3K+G)}$	$K+4G/3$	....
$\frac{EG}{3(3G-E)}$	....	$G\,\frac{E-2G}{3G-E}$	$\frac{E}{2G}-1$	$G\,\frac{4G-E}{3G-E}$	....
....	....	$3K\,\frac{3K-E}{9K-E}$	$\frac{3K-E}{6K}$	$3K\,\frac{3K+E}{9K-E}$	$\frac{3KE}{9K-E}$
$\lambda\,\frac{(1+\nu)}{3\nu}$	$\lambda\,\frac{(1+\nu)(1-2\nu)}{\nu}$	....	....	$\lambda\,\frac{(1-\nu)}{\nu}$	$\lambda\,\frac{(1-2\nu)}{2\nu}$
$G\,\frac{2(1+\nu)}{3(1-2\nu)}$	$2G(1+\nu)$	$G\,\frac{2\nu}{1-2\nu}$	....	$G\,\frac{2-2\nu}{1-2\nu}$	....
....	$3K(1-2\nu)$	$3K\,\frac{\nu}{1+\nu}$	....	$3K\,\frac{1(1-\nu)}{1+\nu}$	$3K\left(\frac{1-2\nu}{2+2\nu}\right)$
$\frac{E}{3(1-2\nu)}$	....	$\frac{E}{(1+\nu)(1-2\nu)}$	....	$\frac{(1-\nu)}{(1+\nu)(1-2\nu)}$	$\frac{E}{2+2\nu}$
$\rho(v_\ell^2-\frac{4}{3}v_s^2)$	$\frac{3v_s^2(v_\ell^2-\frac{4}{3}v_s^2}{(v_\ell^2-v_s^2)}$	$\rho(v_\ell^2-2v_s^2)$	$\frac{1}{2}\left\{1-\left[\frac{v_\ell^2}{v_s^2}-1\right]^{-1}\right\}$	ρv_ℓ^2	ρv_s^2

*After Birch, F., J. Geophys. Res., 66, 2199 (1961).

APPENDIX B

Stress Distribution in a Diametrically Loaded Sphere

An analysis of the stress distribution in a diametrically loaded sphere with a distributed load has been accomplished by Shook.[34] The analysis is analogous to the similar problem of the diametrically loaded cylinder given by Timoshenko and Goodier.[44]

The solutions to the problem of a load distributed over a circular area on a semi-infinite solid (see Figure B-1) are also given by Timoshenko and Goodier as

$$\sigma_z = q\left[-1 + \frac{z^3}{(a^2 + z^2)^{3/2}}\right] \qquad \text{B-1}$$

$$\sigma_r = \frac{q}{2}\left[-(1+2\nu) + \frac{2(1+\nu)z}{\sqrt{a^2 + z^2}} - \left(\frac{z}{\sqrt{a^2 + z^2}}\right)^3\right] \qquad \text{B-2}$$

where, a = radius of the loaded area

z = distance along loaded diameter

r = direction transverse to load

d = diameter of sphere

q = load intensity = $P/\pi a^2$

ν = Poisson's ratio

It has also been shown that a semi-infinite solid under a point contains an effective sphere tangent to the point of loading which experiences a constant compressive stress of $3P/2\pi d^2$ at all points

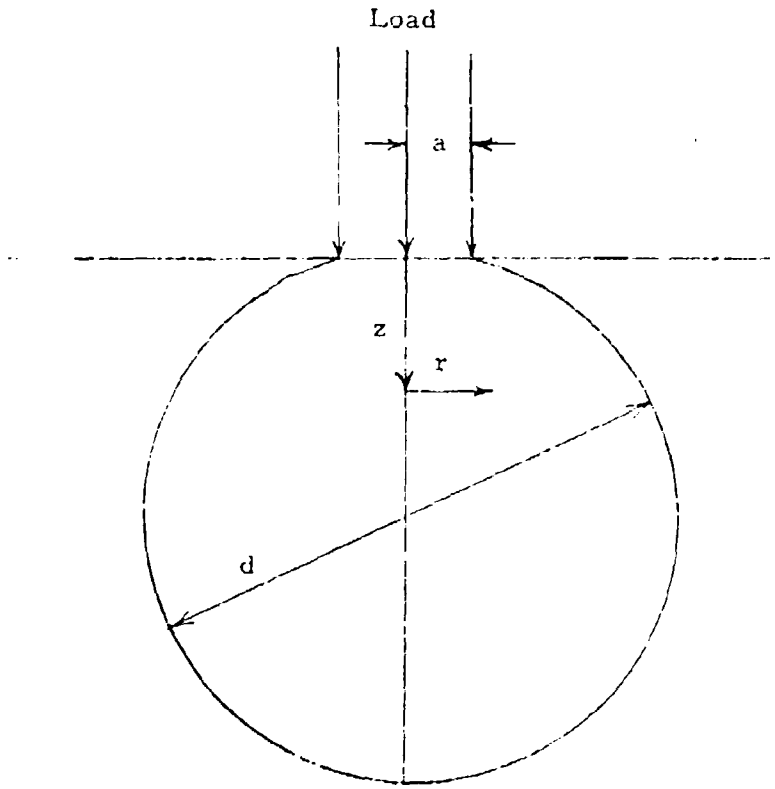

Figure B-1 Illustration for the Problem of a Load Distributed Over a Circular Area on a Semi-infinite Solid.

on its surface. When such a sphere is extracted from the semi-infinite solid there must exist a constant tensile load of $3P/2\pi d^2$ at all points on its surface.

Superpositioning, then, the constant tensile stress on the solution for stresses in the semi-infinite solid, the stresses in a diametrically loaded sphere become

$$\sigma_{z(\text{sphere})}\Big|_{z=cd} = \sigma_z\Big|_{z=cd} + \sigma_z\Big|_{z=(1-c)d} + 3P/2\pi d^2 \qquad \text{B-3}$$

$$\sigma_{r(\text{sphere})}\Big|_{z=cd} = \sigma_r\Big|_{z=cd} + \sigma_r\Big|_{z=(1-c)d} + 3P/2\pi d^2 \qquad \text{B-4}$$

where $0 \leq c \leq 1$. The complete solutions given above must account for the stresses developed by both the top load and the bottom load; thus the two calculations at depths equivalent to the distance to each load point. The distribution of stresses is, of course, symmetrical about the loaded diameter as well as about the plane transverse to the loaded diameter through the center of the sphere.

Figure B-2 shows two sets of curves which describe the radial stress distribution in a diametrically loaded sphere. The curves intersecting the origin indicate the position along the loaded diameter at which the maximum stress occurs for a given loaded diameter to sphere diameter ratio and Poisson's ratio. The other set of curves indicate a dimensionless constant which, when multiplied by the load

and divided by the square of the sphere diameter, predicts the maximum radial stress.

Figure B-2. (After Shook 34)